Synthesis and Characterization of CoCr$_2$O$_4$ Nanoparticles
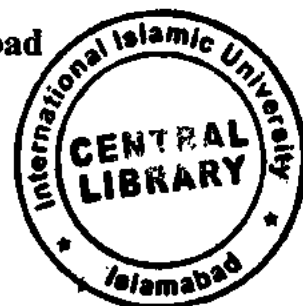
by

Umair Rashid

(239-FBAS/MSPHY/F13)

Supervisor

Dr. Kashif Nadeem
Assistant Professor (TTS)
Department of Physics, FBAS, IIUI

Department of Physics
Faculty of Basic and Applied Sciences
International Islamic University, Islamabad
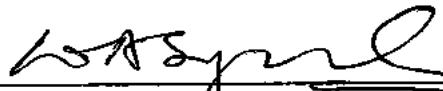
Synthesis and Characterization of $CoCr_2O_4$ Nanoparticles
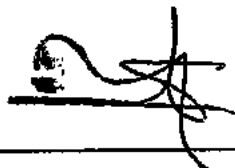
by:

Umair Rashid

(239-FBAS/MSPHY/F13)

This Thesis submitted to Department of Physics International Islamic University, Islamabad for the award of degree of MS Physics.
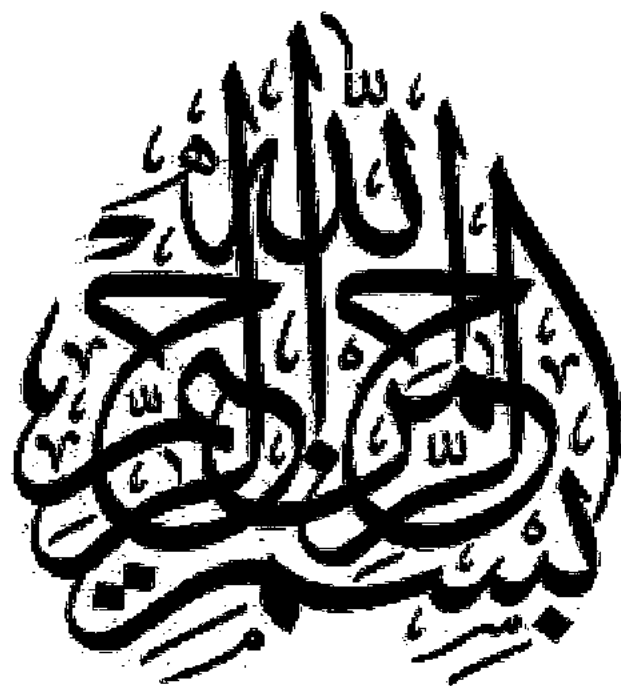
_____

Chairman Department of Physics

International Islamic University, Islamabad.

_____

Dean Faculty of Basic and Applied Sciences

International Islamic University, Islamabad.

بسم الله الرحمن الرحيم

DEDICATED

to

My beloved

Mother

Father

and

My

Respected teachers

Declaration

I **Umair Rashid** (Registration # 239-FBAS/MSPHY/F13), student of MS in Physics (session 2013-2016), hereby declare that the matter printed in the thesis titled "Synthesis and Characterization of $CoCr_2O_4$ nanoparticles" is my own work and has not been published or submitted as research work or thesis in any form in any other university or institute in Pakistan or aboard.
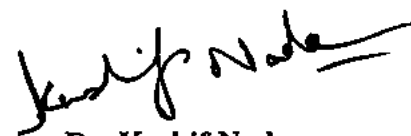
<div align="right">

Umair Rashid

(239-FBAS/MSPHY/F13)

</div>

Dated; 4th April 2016

FORWARDING SHEET BY RESEARCH SUPERVISOR

The thesis entitled "Synthesis and Characterization of $CoCr_2O_4$ nanoparticles" submitted by *Umair Rashid* in partial fulfillment of M.S. degree in Physics has been completed under my guidance and supervision. I am satisfied with the quality of student's research work and allow him to submit this thesis for further process to graduate with Master of Science degree from Department of Physics, as per IIU rules and regulations.

Dated: 4th April 2016

Dr. Kashif Nadeem,
Assistant Professor (TTS)
Department of Physics,
International Islamic University,
Islamabad.

ACKNOWLEDGMENT

First, I owe my deepest gratitude to **Allah** Almighty for all of his countless blessings. I offer my humblest words of thanks to HIS most noble messenger **Hazrat Muhammad (P.B.U.H)**, who is forever, a torch of guidance and knowledge for all humanity. By virtue of his blessings today I am able to carry out our research work and present it.

I would like to acknowledge the worth mentioning supervision of **Dr. Kashif Nadeem** who guided me and supported me during my whole research work. I am also thankful to him as he helped and guided me to complete my research work in time. Moreover, under their supervision from the preliminary to the concluding level enabled me to develop an understanding of the field. Their wide and deep knowledge have been a great value for me. Frankly speaking without effort of **Dr. Kashif Nadeem** it was impossible to complete this hard task of my life. He is always an inspiring personality for me in all fields specially education. He always an enlighten me and guide me at each and every step of my MS. Without his guidance it was not possible for me to complete my MS. Almighty **Allah** blessed them in every part of life.

Moreover, I would like to express my sincere thanks to all the faculty members of Department of Physics IIU Islamabad especially to Dr. Waqar Adil Syed (Chairman). I would also like to thank all other faculty members of my university for their sincere appreciation, comments and suggestions. I express my thanks to all staff of Physics Department, IIU, for their various services. I shall express my heartiest thanks to all my senior research colleagues Dr. Abdul Jabbar, Liaqat Ali, Muhammad Kamran, Asmatullah and Shahzad for being very supportive and co-operative all throughout my research work.

I especially want to acknowledge my elder brother Umer Rasheed, my younger brothers Zubair Rasheed, Muhammad Hamza and my sister Zainab Qamar for their encouragement, support and confidence on me. During my education career their personality will remain the role model for me. Finally I am thankful to my parents for their love, care and support in my life, which has been directly encouraging me for my study. My parent's prayers have always been a big support in solving my problems. Allah may bless my parents and family with long life, health and happiness.

Umair Rashid

Table of Contents

List of Figures

ABSTRACT

Cobalt chromite ($CoCr_2O_4$) nanoparticles dispersed in silica (SiO_2)$_x$ matrix (x = 0, 45, 60 and 80 wt. %) were prepared by using sol-gel method. Influence of SiO_2 matrix on structural and dielectric properties of $CoCr_2O_4$ nanoparticles have been discussed in detail. Using X-rays diffraction (XRD) analysis crystallite size turn out to be in the range of 30-67 nm and the crystal structure of nanoparticles is cubic spinel. Average crystallize size of these nanoparticles was calculated by using Debye-Scherrer formula. Both average crystallite size and lattice constant were decreased with increasing SiO_2 concentration, which indicates that SiO_2 (non-magnetic) restricts the growth of nanoparticle. SiO_2 is used as a spacer to avoid agglomeration of nanoparticles. Ultra-Violet (U-V) spectroscopy proved the formation of spinel chromite. Transmission electron microscopy (TEM) images revealed that the nanoparticles are non-agglomerated due to surface coating of non-magnetic SiO_2. The magnetization curve of zero field cooled (ZFC) and field cooled (FC) for $CoCr_2O_4$ were obtained under applied magnetic field of 50 Oe with paramagnetic to ferromagnetic transition temperature (T_c) = 97 K and conical spin transition (T_s) = 30 K. Dielectric constant and tangent loss were decreased with increasing frequency and becomes constant for higher frequencies. However conductivity revealed opposite trend and has greater values at higher frequencies. Dielectric properties have been explained by using Koop's theory and tangent resonance phenomena. Dielectric properties also showed dependence on the SiO_2 concentration. Hence, these measurements indicated that the structural and dielectric properties of $CoCr_2O_4$ nanoparticles strongly depend on SiO_2 concentration.

CHAPTER 1

Introduction

1.1 Magnetism Overview

The word magnetism comes from the state of "Magnesia". About 2000 years ago, Greeks found some stones which have property to attract iron pieces. The compass was designed by the magnets and then magnets were used for navigation by the Chinese in the 12th century. With the passage of time people thinking about the nature of magnets and the reason behind attraction of iron pieces. After the developments of atomic model an idea about the nucleus and electronic shells was found with the concept of electrons having two types of motion one is the orbital motion other is the spin motion. Then came to this point that the electronic interaction, spin and orbital motion of electrons is responsible for the origin of magnetism [1].

1.2 Origin of Magnetism

It's the fundamental property of an electron that it has a magnetic dipole moment. Each magnetic moment acts as a tiny magnet. Dipole moment is the result of quantum mechanical spin of electrons. Because of its quantum nature, the spin of the electrons can have only two states i.e. 'up' or 'down'. The main source of magnetism is the spin of electrons in atom as well as orbital motion of electrons around the nucleus. If these magnetic dipoles are aligned in a piece of matter and point in the similar direction, their discrete tiny magnetic fields add together to create a stronger external magnetic field.

However, those materials whose atoms have completely filled electronic shell carry zero dipole moment, because magnetic moment of every electron is cancelled by the opposite moment of the second electron in the pair. Those atoms whose shells are partially filled (i.e. unpaired spins) can have a definite magnetic moment. Therefore, atoms with partially filled electronic shells are likely to get ferromagnetic nature [2].

1.3 Types of Magnetic Materials

On the basis of magnetic properties, following are the types of materials

> ➤ Diamagnetic materials
> ➤ Paramagnetic materials
> ➤ Ferromagnetic materials
> ➤ Antiferromagnetic materials
> ➤ Ferrimagnetic materials

1.3.1 Diamagnetic Materials

Diamagnetic materials are those in which there is no net magnetic moments of atoms, but show a week, negative susceptibility to external magnetic field. However magnetization is zero in the absence of magnetic field. Diamagnetic properties are actually due to complete electronic shells of the atoms. When exposed to external magnetic field they oppose that effect. Few diamagnetic materials are gold, silver and copper [3].

1.3.2 Paramagnetic Materials

In the absence of an external field, the paramagnetic material exhibits no net magnetization. In this class of materials the magnetic moment is non-zero for each atom, but their combined average is zero. As soon as we apply external magnetic field magnetic moments align in the same direction as that of field, which results in a net positive magnetization. These materials do not show any hysteresis. Paramagnetic materials take account of magnesium, aluminum, molybdenum, lithium, and tantalum [4].

1.3.3 Ferromagnetic Materials

Ferromagnetism can be said as a special case of paramagnetism where the individual spins of moments interact individually. The unremunerated spins in individual atoms of a ferromagnetic material may couple directly known as direct exchange. Parallel alignment of moments occurs in ferromagnetic materials which results in large net magnetization even when there is no magnetic field. This spontaneous magnetization is called net moment. The ferromagnetic materials become paramagnetic above the Curie temperature due to vanishing of spontaneous magnetization. For example iron becomes paramagnetic at 750°C [5]. Few examples of ferromagnetic materials are cobalt, iron and nickel.

1.3.4 Ferrimagnetic Materials

In ferrimagnetism, the exchange interaction is negative (antiferromagnetic) but carries some resultant magnetic moment. Magnetic oxides are the chief sources of ferrimagnetic materials also known as ferrites. Naturally occurring chromium is in two states compound

Chromium (II) ions, Cr^{2+}, and Chromium (III) ions. In $CoCr_2O_4$ there is a negative oxygen ions in O^{2-} and positive chromium in Cr^{3+} state. The oxygen ions are not magnetic, but both chromium ions are. In the given crystals, chemically formulated as Cr_3O_4, for every four oxygen ions there are three Cr^{3+} ions. Fig 1.1 shows magnetic ordering of ferromagnets, antiferromagnets and ferrimagnets.
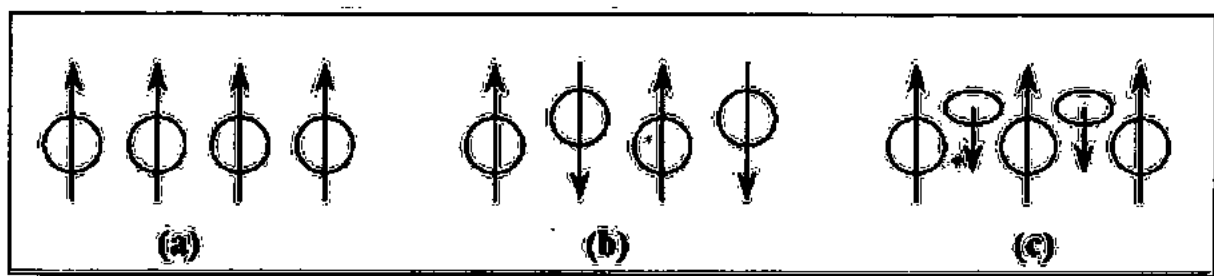
Fig. 1.1: Magnetic ordering (a) Ferromagnet (b) Antiferromagnet (c) Ferrimagnet.

In the present work we will discuss about the ferrimagnetic material $CoCr_2O_4$. It has all the properties of ferromagnetic response such as hysteresis, remanence and Curie temperature. However ferromagnetisms, antiferromagnets and ferrimagnet have different magnetic arrangement [6]. Fig 1.1 shows ferromagnet, antiferromagnet and ferrimagnet schematic.

1.3.5 Antiferromagnetic Materials

If magnetic moments of every two neighboring sub lattice are equal but opposite, the net magnetic moment will be zero. This type of magnetic arrangement is called antiferromagnetism. These materials too have no hysteresis yet there is small positive susceptibility [7].

1.3.6 Dielectric Polarization

Dielectrics are bad conductors of electricity. In the presence of external electric field, its electric lines of force always originate from positive charges and terminate at negative charges. Charges do not flow through the dielectric. Positive charges means shifting of nucleus in the direction of electric field and negative charges means electrons are shifted in the opposite direction (because of the electrostatics effects) and this phenomenon is known as dielectric polarization as shown in Fig. 1.2
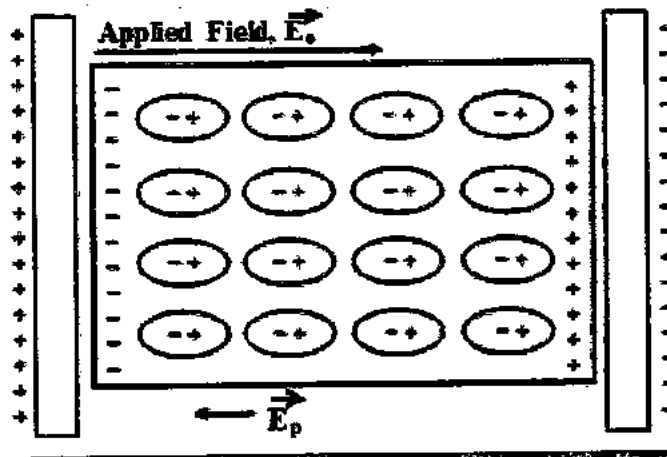
Fig. 1.2: Polarization of dielectric material [8].

As a result of these displaced charges, an electric field is produced which is opposite in direction of the external field applied, known as polarization field. Net electric field across the dielectric is reduced because of the polarization field. While dielectric is placed between the capacitor plates, charge storage in the dielectric improves. Dielectric polarization is summarized as "the dipole moment per unit volume" and can be written as;

$$\vec{P} = \frac{\Sigma p}{V} \tag{1.1}$$

1.3.7 Susceptibility, Permittivity and Dielectric Constant

For the case of linear dielectric materials, polarization depends on the electric field E, provided E is weak field i.e.

$$P = \epsilon_0 \chi E \tag{1.2}$$

The constant of proportionality χ is called the electric susceptibility of a medium. The electric dielectric vector of the medium is defined as

$$D = \epsilon_0 E + P = \epsilon_0 E + \epsilon_0 \chi E = \epsilon_0 (1 + \chi) E = \epsilon E \tag{1.3}$$

where

$$\epsilon = \epsilon_0 (1 + \chi) \tag{1.4}$$

$\epsilon_0 = 8.85418782 \times 10^{-12}$ F/m.

4

The dielectric constant or relative permittivity [9] is defined as,

$$\epsilon_r = 1 + \chi = \frac{\epsilon}{\epsilon_0} \qquad (1.5)$$

1.4 Nanoscience

Nanoscience involves the study of process and preparation of materials at atomic and molecular levels. Properties of materials at nanoscale are totally different at bulk scale due to the high surface to volume ratio at nanoscale.

1.4.1 Nanotechnology

Technology that deals with the particle size in the range of 1 to 100 nm is called nanotechnology. Nanotechnology involves designing, characterization and preparation by defining its structure of material and devices, and system by controlling shape and size of material.

1.4.2 History

Nano is a Greek word which means dwarf. The idea of nanoscience and nanotechnology was given first time by Richard Feynman in 1959 [10]. Term 'nanotechnology' was first used by a scientist Norio Taniguchi of Tokyo University in 1983 [11]. There is difference of size, shape and properties between nanomaterials and bulk materials.

1.4.3 Introduction to Nanotechnology

One billionth of meter is called nanometer, numerically (10^{-9}). Nanomaterials have high surface to volume ratio which make materials prominent at nanoscale. For example single atom in case of metal is non-conducting but bulk metallic materials have conducting nature. Materials become more significant when its size decreases at nanometer range. Materials have very promising properties in case of 1-dimensional, 2-dimensional and 3- dimensional with nanometer (nm) range. So properties of these materials are not similar as that of bulk materials [12]. As size of material decreases to less than 50 nm its surface area to volume ratio increases significantly. Magnetic memory of nanomaterial depends upon its size [13]. Fig. 1.3 shows SEM images of some 1dimensional nanomaterials
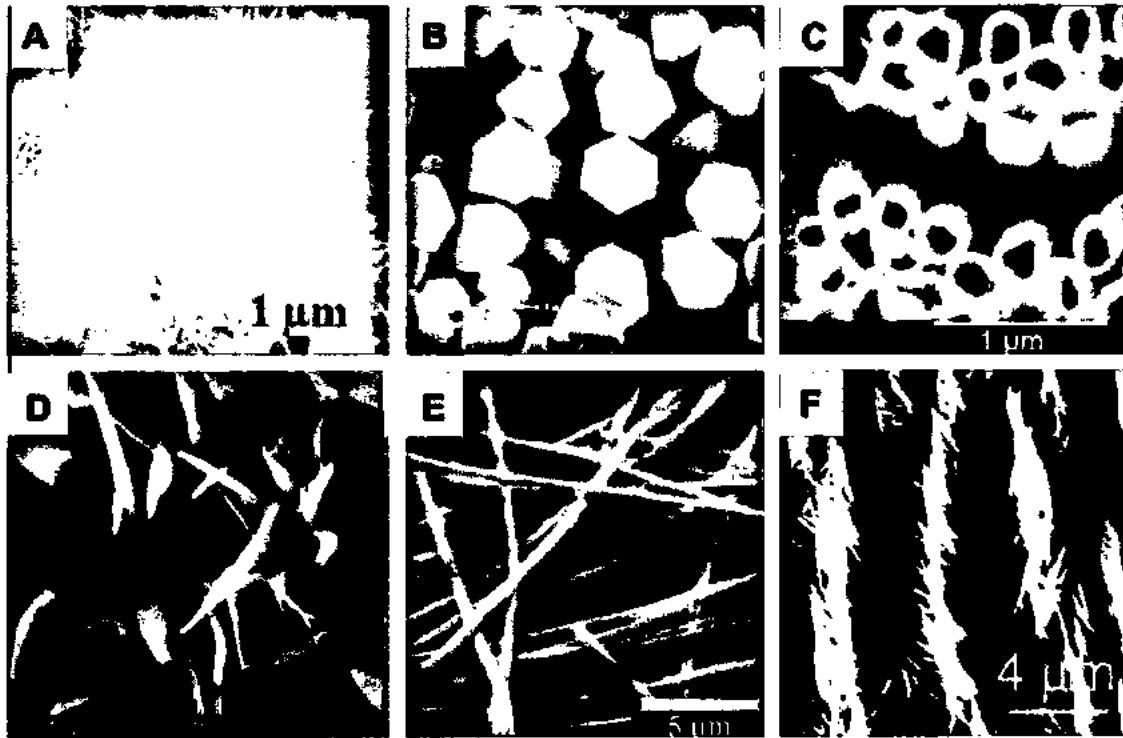
Fig. 1.3: Typical SEM images of different types of 1-dimensional nanomaterials [14].

1.4.4 Nanoparticles

These are the particles having a diameter in range of 1-100 nm. Nanoparticles can be in the form of nanocrystals, clusters and colloids. Nanoparticles have got unique properties which are different from their bulk states. With the decrease in size of nanoparticles, there electrical, mechanical, optical and other properties are changed drastically.

Magnetic properties of nanoparticles are also different from their bulk states. When size of particles decreases to less than 100 nm then ferromagnetism of nanoparticles changes to superparamagnetic due to larger surface to volume ratio which enhance surface energy of nanoparticles [15].

1.4.5 Nanomaterials

Material particles with size from 1 to 1000nm are normally termed as nanomaterials. Here is the list of some nano-sized materials. Two principal factors which causes the characteristics of nanomaterials to differ from bulk materials are,

- Increased relative surface area
- Quantum effects

Conventional material have grain size 100nm to 100μm. Here are few examples of nano-sized materials listed in Table 1.0,

Table 1.0: Small sized material and their actual size in nano scale [16].

Material	Size in nanometer
Animal hair	30,000 nm
Molecules with 20 atoms	1 nm diameter
Human cells	1000 –100,000 nm
Proteins	2-40 nm
Viruses	5-400 nm

1.4.6 Chromites

By definition, chromite is a type of a ceramic compound composed of chromium oxide (Cr_2O_4) chemically combined with one or more supplementary metallic elements. Its general formulae is XCr_2O_4; their character is ferromagnetic.

Chromites with $A^{2+}Cr^{3+}O_4^{2-}$ formula are binary oxides, where A^{2+} and Cr^{3+} occupies tetrahedral (A) and octahedral (B) sites respectively. There are number of potential applications of chromites ranging from semiconductors, high-temperature ceramics, and catalysts to electrochemical sensors. In our research we used chromite as $CoCr_2O_4$ [17].

1.4.7 Structure, Bonding and Classification of CoCr₂O₄

Spinels have got general formula AB_2X_4. They have many applications in nanoscience and technology [18-21]. For example, chromites XCr_2Y_4; X =Fe, Ni, Mg etc., Y=S, O ions exhibit many rare magnetic properties such as ferrimagnetism, colossal magnetoresistance, etc. In $CoCr_2O_4$, Co^{2+} ions are in tetrahedral (A) sites and Cr^{3+} ions are in octahedral (B) sites [22] $(Co^{2+})_t$–$(Cr^{3+})_o$–O_4. It is a ferrimagnetic system. In spinel structure of collinear ferrimagnetic system, A-O-B and B-O-B bond angle are 125° and 90°, correspondingly. For other

7

configurations, J_{AB} super exchange interactions are unlikely to appear. J_{BB} C--O—Cr interactions in chromite control its magnetic properties. Therefore, spiral ferrimagnetic arrangement might dominate the magnetic order; just because the collinear model finds incorrect [23-25]. The antiferromagnetic arrangement between A and B sites is totally demolished in $CoCr_2O_4$, and the system shows a screw ordering. This is known as "ferrimagnetic spiral" [26-28]. Recently, single crystals of $CoCr_2O_4$ have shown to be a unique multiferroic materials i.e. the spiral component induces the observed electric polarization P and also has a spontaneous magnetization M [29, 30]. However, the studies have been mostly focused on single and bulk crystals of $CoCr_2O_4$ except in one report which deal with polycrystalline samples. Both single crystals as well as polycrystalline samples of $CoCr_2O_4$ develop ferrimagnetic order having long-range below Tc=94 K, and a sharp phase transition at Ts=26 K. Reports on dielectric properties of nano-crystalline $CoCr_2O_4$ are scarce and the studies are mostly focused on the field dependence of magnetization at low temperature.

CHAPTER 2

Synthesis and Literature Review

2.1 Literature Review

Nanoparticles of chromites have got special attention to researchers and scientists due to their novel properties. Properties of chromite nanoparticles can be tuned easily through different synthesis techniques and different substitutions. Lots of work has been done on different substitutions, synthesis techniques, temperature dependence and magnetic properties etc. As we searched there is not much data found on size effects on dielectric properties so we worked on that project. This work is novel because nobody else have done this before for these samples. Broad study of dielectric and electrical properties on a series of silica substituted $CoFe_2O_4$ were made done. The particle size decreases with the increase in concentration of SiO_2 matrix. This decrease of size was due to replacement of silicon ions of smaller radius instead of larger radius of iron ions.

1. The coating of SiO_2 on potassium ferrite ($KFeO_2$) nanoparticles has been reported in the given paper [31]. The XRD exposed the formation of orthorhombic structure of uncoated potassium ferrite nanoparticles which was also retained after the SiO_2 coating. After coating it was found that Si coated material have got more stability. In VSM analysis, both bare potassium ferrite exhibits more magnetic saturation value than the coated potassium ferrite. This decrease in size is due to the creation of magnetically dead layer of SiO_2 which reduces the diameter of the particles as compared to its physical size. The thermal decomposition of SiO_2 coated potassium ferrite nanoparticles exhibits a weight loss accompanied with an exothermic peak, pertaining to the condensation of silanol in the SiO_2 matrix. The SiO_2 coated potassium ferrite nanoparticles exhibit increased viability as compared to bare nanoparticles; attributed to the good dispensability and reduced agglomeration due to SiO_2 coating.

2. SiO_2 coated $Co_{1-x}Zn_xFe_2O_4$ nanoparticles with concentration of x as 0, 20%, 30%, 40%, 50%, and 100% were synthesized by using sol–gel method [32]. XRD was used for the structural studies. SEM and FTIR was used for morphological studies. XRD results showed cubic spinel structure for all the examined samples. The average size of crystals turned out

to be in the range of 36–47 nm. The lattice constant increases with the increase of Zn concentration because of large ionic radii of Zn^{2+} in contrast to Co^{2+} ions. FTIR spectroscopy showed the presence of SiO_2 coated ferrite nanoparticles. SEM images revealed that the nanocrystals are in thin size, spherical in shape and non-agglomerated due to coating of SiO_2 shell. It was then confirmed that the structural and magnetic properties of SiO_2 coated $Co_{1-x}Zn_xFe_2O_4$ ferrite nanoparticles intensely depend upon the average crystallite size and concentration of Zn^{2+} ions.

3. Nanoparticles of $CoFe_2O_4$ were synthesized *in situ* with the addition of SiO_2 matrix using sol–gel method [33]. The magnetic properties of the particles were inspected by varying the weight ratio of $CoFe_2O_4$. Structural properties depend on variation in annealing temperature. The samples with 45 wt. % cobalt ferrite sintered at 875 K and above were indicated as a single phase spinel structure. Its nature was found to be 'ferrimagnetic'. Nevertheless, the samples which were annealed below 775 K showed superparamagnetic behavior. It was initiated that coercivity (H_c), magnetization (M_s) and maximum remanent magnetization (M_r) increases uniformly with sintering temperature and with the corresponding saturation of 21.09 emu g^{-1}, 5.671 emu g^{-1} and 1.15 kOe, respectively. The samples sintered at 1073 K were ferromagnetic in nature, excluding one with 10 wt. % cobalt ferrite, as it is superparamagnetic. The respective maxima was 33.28 emu g^{-1}, 11.41 emu g^{-1} and 1207 Oe, respectively. The M_s and M_r increases with content of cobalt ferrite, except for the value of H_c.

4. Sol–gel method was used to synthesize superparamagnetic and ferromagnetic $CoFe_2O_4/SiO_2$ nanocomposites by changing the weight percentage or annealing temperature of cobalt ferrite [34]. From XRD investigations it was evident that SiO_2 plays a vital role in controlling the average crystallite size. Mossbauer spectra showed the mixed spinel structure of cobalt ferrite nanocomposites. Size of the maximum spinel particles is as small as to retain the ferromagnetic properties, same is the reason of super paramagnetic behavior of particles. The average crystallite size of $CoFe_2O_4/SiO_2$ nanoparticles were about 12 nm.

5. $NiFe_2O_4$ nanoparticles (5–33 nm) were synthesized using co-precipitation technique [35]. To prepare core–shell nanocomposite, they were coated with SiO_2 following the Stöber process. X-ray diffraction analysis was used to obtain phase and average particle size. Scanning electron microscope was employed to study particle size distributions and transmission electron microscope analyzed morphology of core-shell nanoparticles. FTIR

gave identification about the presence of bonds in the uncoated and coated samples. Superparamagnetic properties were measured at room temperature when the uncoated crystallite size was 15nm or less than that. The blocking temperature increases with increasing particle size and T_b was lesser for coated samples as compared to the corresponding uncoated samples. FESEM confirmed core diameter size was much larger than the uncoated ones [35].

6. Cobalt ferrite ($CoFe_2O_4$) having a non-magnetic shell of SiO_2 were prepared using sol-gel method [36]. The structural properties and magnetic characteristics were then examined. The results indicated that single phase $CoFe_2O_4$ coated with SiO_2 can be partially formed when the dried gel is sintered at temperature above 400°C. These grains were detected to intermingle with the matrix through Si–O–Fe bonds. When the temperature is increased up to 600°C, that interaction reaches its maximum value, particles of Co-ferrite grains developed into nanocrystals, whereas the interaction between the SiO_2 matrix and Co-ferrite clusters vanished with the splintering of the Si–O–Fe bonds. The average particle size could be checked by the Co-ferrite content and variation of annealing temperature. At low temperature, remanent magnetization and coercivity decreases with the increase of measuring temperature. The magnetization saturation values increases by increasing quantity of SiO_2 in $CoFe_2O_4$.

7. Gingasua et al. [37] prepared $CoCr_2O_4$ through the precursor method. Raman spectroscopy were used to classify final oxides. XRD authenticated the cubic $CoCr_2O_4$ phase only. Average crystallite sizes lies in a range between 14 and 21 nm. Scanning electron microscopy revealed cubic structure of $CoCr_2O_4$ crystals. All the samples exposed ferrimagnetic nature below the Currie temperature, and a phase transition at Ts~27 K attributed to the outbreak of long range spiral magnetic arrangement. The $CoCr_2O_4$ nanoparticles synthesized through the gluconate route and calcined at 700°C for 1 h were found that they became more catalytic [38].

8. Dutta et al. [39] prepared $CoCr_2O_4$ nanoparticles by sonochemical technique. $CoCr_2O_4$ is a multiferroic material. X-ray diffraction method, transmission electron microscopy and scanning electron microscopy were used to find structural properties, morphology and particle size of the $CoCr_2O_4$ nanoparticles. Whereas superconducting quantum interference device magnetometer was used to distinguish temperature dependent magnetic transitions. The bulk $CoCr_2O_4$ exhibits two magnetic transitions, T_c~98 K and T_s~26 K, the nanoparticles here showed a T_c~84 K and T_s~25 K. Magnetic studies on the nanoparticles indicated the presence of long-range ferromagnetic order below 84 K and also another

transition temperature 25 K corresponding to the beginning of spiral magnetic order. Since the onset of ferroelectricity in $CoCr_2O_4$ nanoparticles matches the spiral magnetic ordering transition, it will be of great interest to study the influence of size of the nanoparticles on its overall multiferroic nature.

9. Nadeem *et al.* [40] carried out the effects of SiO_2 concentration on dielectric properties of cobalt ferrite nanocomposites with concertation of SiO_2 10%, 30%, 50% and 60%. Due to greater number of nucleation sites generated by SiO_2, size of particles restricted. With the increase of frequency, dielectric properties such as dielectric constant, imaginary part, loss factor and AC conductivity decreases. All dielectric parameter shows that they depend on concentration of SiO_2. Thus SiO_2 matrix is quite useful in decreasing particle size. The reason behind reduction of crystallite size is the enlargement of surface area and shrinkage of volume. Real dielectric values of bulk samples are much smaller than the experimental results of coated nano samples which showed that grain size reduces. At higher values of frequency polarization is small and conductivity is large, and conductivity gets decrease at lower frequencies where the polarization is maximum.

2.2 Synthesis of $CoCr_2O_4$ nanoparticles embedded in SiO_2

Now I shall discuss the synthesis technique used to prepare $CoCr_2O_4$ nanoparticles and their structural characterization via X-ray diffraction (XRD).

2.2.1 Sol-gel Technique

There are various methods for the preparation of nanoparticles. Among all of them wet chemical route is the one which gives better especially to provide low processing temperature, smaller particle, size etc. The preparation of nanoparticles from a solution of chemical compounds can be divided into following major categories,

1. Colloidal methods.
2. Sol-gel processing.
3. Water-oil micro emulsion method.
4. Hydrothermal synthesis.
5. Polyol method.

Among all the methods listed above sol-gel [41] is a well-known and widely used synthesis technique for the preparation of nanoparticles. Some of the advantages and disadvantages of this technique are given below.

2.2.1.1 Advantages

- Control over the molar fraction.
- Materials with various compositions can be prepared.
- Impurity phases can be avoided by controlling various parameters.
- Size distribution of the nanoparticles can be controlled.
- It is relatively simple and cost effective.

2.2.1.2 Disadvantages

- High concentration of raw materials.
- Long processing time.

Recently, there has been a great interest for the synthesis and development of diluted magnetic semiconductor (DMS) nanoparticles from chemical methods; given that direct chemical approaches are generally compatible with large-scale production and the resulting colloidal suspensions are ready for application in self-assembly strategies that have become a foundation of nanotechnology [42].

2.2.2 Types of Sol-gel Technique

Sol-gel technique is divided into two categories

- Aqueous sol-gel process.
- Non-aqueous sol-gel process.

2.2.2.1 Aqueous Sol-gel Process

The chemistry of aqueous sol-gel technique is quite complex, on one side there is a high reactivity of water with precursors, and water behaves as a ligand as well as solvent. On the other side there are large number of reaction parameters which have to be controlled such as, temperature, pH, rate of oxidation, nature and concentration of anions etc. Due to low temperature during the synthesis, there is a limitation of aqueous sol-gel chemistry which yields particles being amorphous. Hence this method requires a post-annealing to induce crystallization. Due to this we have to compromise over the crystal size and shape.

2.2.2.2 Non-aqueous Sol-gel Process

This technique takes place in organic solvents. Organic components of solvents play multiple roles in the reaction. They are solvent, surfactants and also act as provider of oxygen for the oxide formation. The reaction rate is slow due to the moderate reactivity of the oxygen-carbon bond and due to this the size and shape of the particles can be controlled. Term non-aqueous synthesis does not imply that water molecules do not take part in reaction, in some of the cases hydrated precursors of metal oxide are used and water is produced during the reaction, therefore a hydrolytic reaction pathway may not be omitted. For example, if the synthesis is achieved with dehydrated zinc acetate (no water molecules) and anhydrous ethylene glycol, no zinc oxide is formed. But when zinc acetate dehydrate (two water molecules) and ethylene glycol are used, zinc oxide is formed [43]. There are two approaches which are used for non-aqueous processes.

- Surfactant-controlled approaches.
- Solvent-controlled approaches.

In surfactant-controlled synthesis, surfactants are used. The surfactants are organic compounds, these surfactants provide a dynamic organic capping layer which enhances their growth and stabilizes the nanoparticles in solution. Solvent-controlled synthesis involves the use of organic solvents. They act as reactants and controlling agent for particle growth. The solvent-controlled approach is simple and contains components i.e. metal oxide precursor and an organic solvent, also there are very low number of by-products.

2.2.3 Chemicals Used for CoCr$_2$O$_4$ Nanoparticles

Chemicals used for synthesis of CoCr$_2$O$_4$ nanoparticles are listed below in the table.

Table 2.2: Chemicals used in synthesis of CoCr$_2$O$_4$.

Formula	Chemicals	Purity	Molecular Weight(g/mol)
Cr(NO$_3$)$_3$.9H$_2$O	Chromium Nitrate	98.1%	400.14
Co(NO$_3$)$_2$.6H$_2$O	Cobalt Nitrate	97.9%	291.02
C$_6$H$_8$O$_7$.H$_2$O	Citric Acid	98.5%	210.13
SiC$_8$H$_{20}$O$_4$	TEOS	99.0%	208.32

I used SiO$_2$ matrix to avoid inter-particle magnetic interactions which can influence their other properties. I used chemical method which is known as sol-gel method for the preparation of these nanoparticles using cobalt nitrate (Co(NO$_3$)$_3$.9H$_2$O), chromium nitrate Cr(NO$_3$)$_3$.9H$_2$O with purity of 98.1%, citric acid (C$_6$H$_8$O$_7$.H$_2$O) with purity of 98.5%, tetra ethyl orthosilicate (TEOS) with purity above 99%, ethanol, ammonia, and distilled water.

❖ CoCr$_2$O$_4$ nanoparticles/SiO$_2$ (0%)

❖ CoCr$_2$O$_4$ nanoparticles/SiO$_2$ (45%)

❖ CoCr$_2$O$_4$ nanoparticles/SiO$_2$ (60%)

❖ CoCr$_2$O$_4$ nanoparticles/ SiO$_2$ (80%)

Annealing temperature for all these samples was 900°C at 4 hrs.
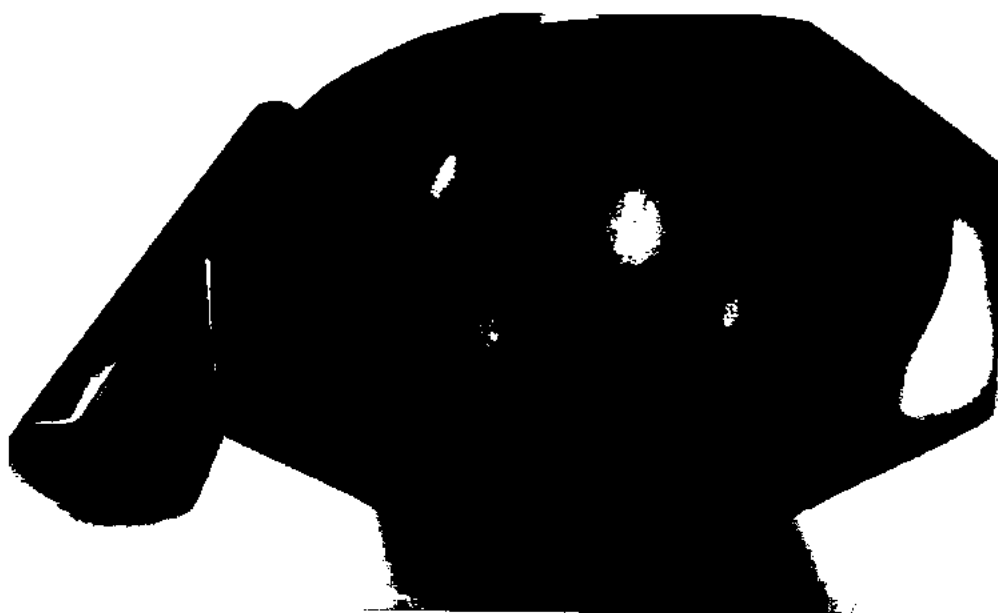
Fig. 2.1: Powder form of grinded sample after annealing.

The general reaction is

$2Cr(NO_3)_3.9H_2O + Co(NO_3)_2.6H_2O + XC_6H_8O_7.H_2O$

$CoCr_2O_4 + YH_2O + N_2 (gas) + ZCO_2 (gas)$
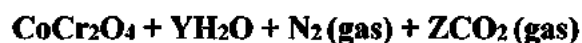
For x = 0.45

TEOS = 3.949 ml

H_2O = 1.27 ml

For x = 0.60

TEOS = 5.26 ml

H_2O = 1.6934 ml

For x =0.80

TEOS =7.02 ml

H_2O =2.26 ml

2.2.4 Sample Preparation

I started the process by measurement of weight of required materials using electronic balance. I put 6 g of chromium nitrate ($Cr(NO_3)_3.9H_2O$) in a beaker and mixed 20 ml of ethanol in that beaker, then put 2.18 g cobalt nitrate $Co(NO_3)_2.6H_2O$ in the same beaker and placed this beaker on magnetic stirrer for continuous stirring. This is called solution 1. In another beaker, I took citric acid ($C_6H_8O_7.H_2O$) of about 4.3 g; molar ratio of nitrates to citric acid = 1:1. After mixing 20 ml of distilled water it is placed on another beaker for stirring purpose to obtain homogenous mixture, this is called solution 2. After few minutes solution 2 is added into mixture of solution 1 dropwise to get main combined solution and this main solution is put on magnetic stirrer to obtain uniform and homogenous mixture. TEOS and water are added after few minutes later into main solution. For 0% sample no TEOS are added. For 45% sample 3.949 ml of TEOS and 1.27 ml of water are added in main solution. In case of 60% sample amount of TEOS and water added are 5.26 ml and 1.6934 ml respectively. For 80% solution TEOS is added with quantity of 7.02 ml and 2.26 ml of water is added in main solution. Fig.

2.2 represents samples of CoCr$_2$O$_4$ nanoparticles with different concentrations of SiO$_2$ after annealing.

After mixing of TEOS and water in main solution, pH value is examined, and then ammonia is added in the same solution until we obtain pH equal to 5. After getting pH value by 5, heating is started using 'heat iron' and temperatures is checked after regular interval of time, and note the temperature all time. Maximum temperature given to sample is 70°C to 80°C and in some sample close to 80°C. Slowly formation of gel started and after some time gel is formed. After gel formation, sample is removed from heating, put this sample in microwave oven at 100°C for 12 hrs. After removing sample from microwave oven, sample is grinded by mortar and pestle. Sample is kept in furnace at 900°C for sintering purpose for 4 hrs. Sample is again removed and grinded again, finally transfer this sample in sample bottle. Fig. 2.2 shows finally prepared samples in bottles.
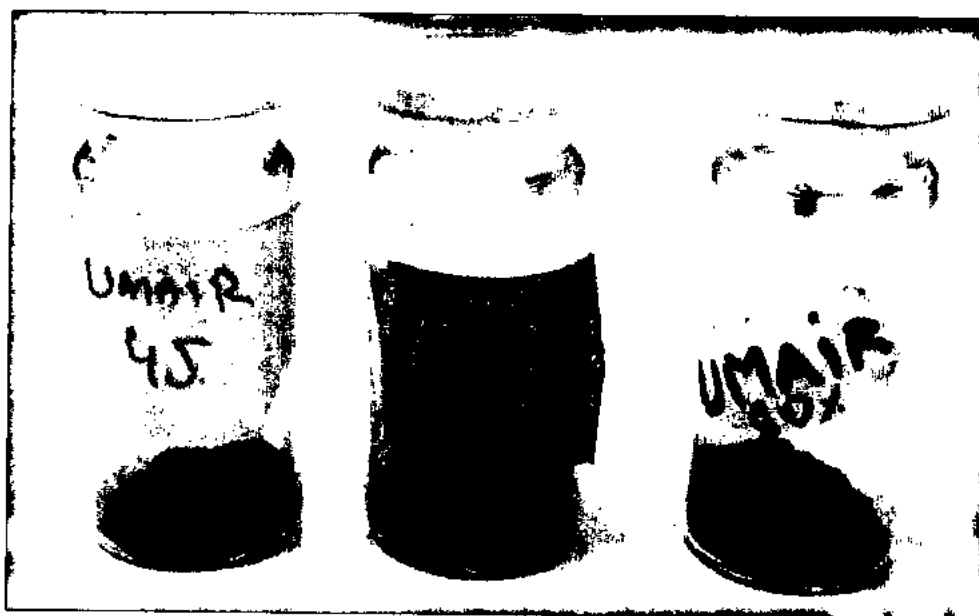
Fig. 2.2: CoCr$_2$O$_4$ nanoparticles samples with 40, 60 and 80% SiO$_2$ matrix

2.2.5 Flow Chart

Flow diagram of the synthesis of cobalt chromite nanoparticles is shown as.

Synthesis of $CoCr_2O_4$ Nanoparticles

Chromium Nitrate → Ethanol ← Cobalt Nitrate

Citric Acid +Water +TEOS → Stirring ← Ammonia for pH control

Stirring at 70°C until gel formation

Dry gel at 100°C over night

Grinding dried gel so as to make powder

Annealing at 900° C for 4 h.

Cobalt chromite in SiO_2 matrix
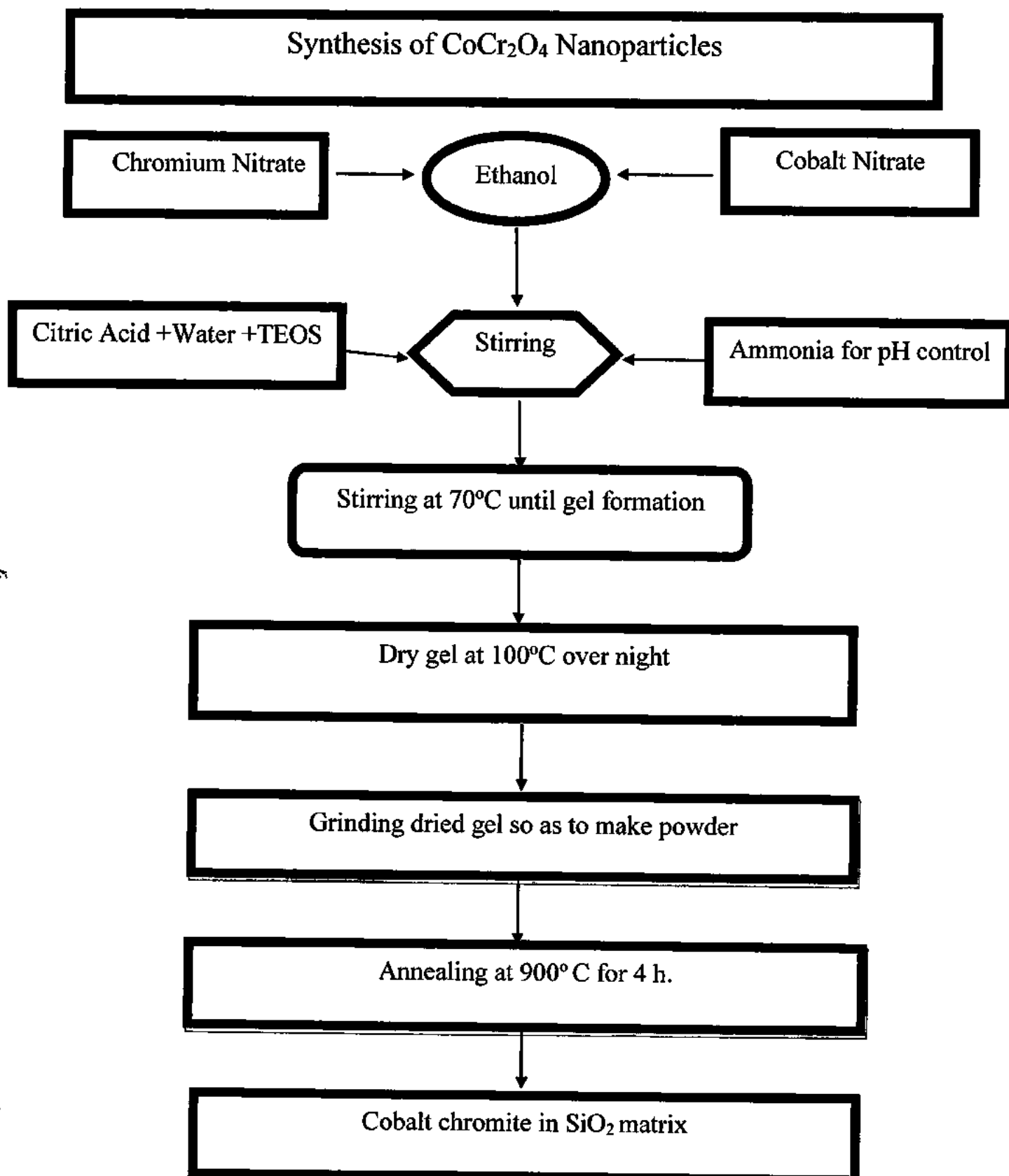
CHAPTER 3

Experimental Techniques

3.1 X-ray diffraction (XRD)

X-ray diffractometer is used for the investigation of the identity of crystalline solids based on the atomic structures of their crystals and angles at which diffraction occurs in powder samples.

3.1.1 Principle of Operation

X-ray diffraction instrument is based on Bragg's law of diffraction.

$$n\lambda = 2d \sin \theta \qquad\qquad (3.1)$$

Using X-ray Diffraction (XRD) technique, the sample is exposed with fixed wave-length (0.1518 nm) and intensity of X-rays. A detector is used for the detections of the reflected radiations. In this technique incoming monochromatic X-rays are diffracted from the crystal for every d-spacing (inter planer spacing) at some specific angles the Bragg's condition will be satisfied by the incoming monochromatic X-rays. In the case of constructive interference we get the XRD peaks otherwise no peak is observed.

3.1.2 Measurements and Verification of the Structure

We used an X-ray diffractometer for the confirmation of the crystal structure (required phase) and the average crystallite size. This diffractometer is powder type and X-rays are CuKα with a wavelength of 1.5406 Å. A sample 'S' in the form of a smooth glass to make it easy for rotation about the axis; this axis being normal to the plane of the glass slide. The X-ray beam with wavelength 1.5406Å, is generated at point and a counter is used for detection of the intensities of the diffracted beams. The X-ray source, specimen, and counter must be coplanar.
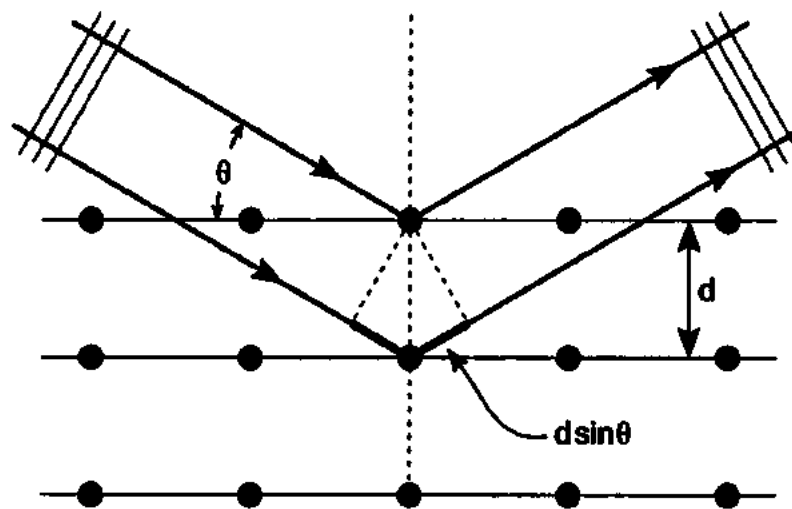
Fig. 3.1: Diffraction and interference of X-rays [44]

The counter is fixed on a moveable carriage; a graduated scale is used for the angular position in terms of 2θ. The specimen and the carriage are mechanically attached in such a way that a rotation of the specimen with horizontal axis through θ is supplemented by a rotation of the counter (2θ) with horizontal axis, as this declares that the incident and reflected angles are kept similar to one another.

Fig. 3.2: Schematic representation of X-ray diffractometer [45].
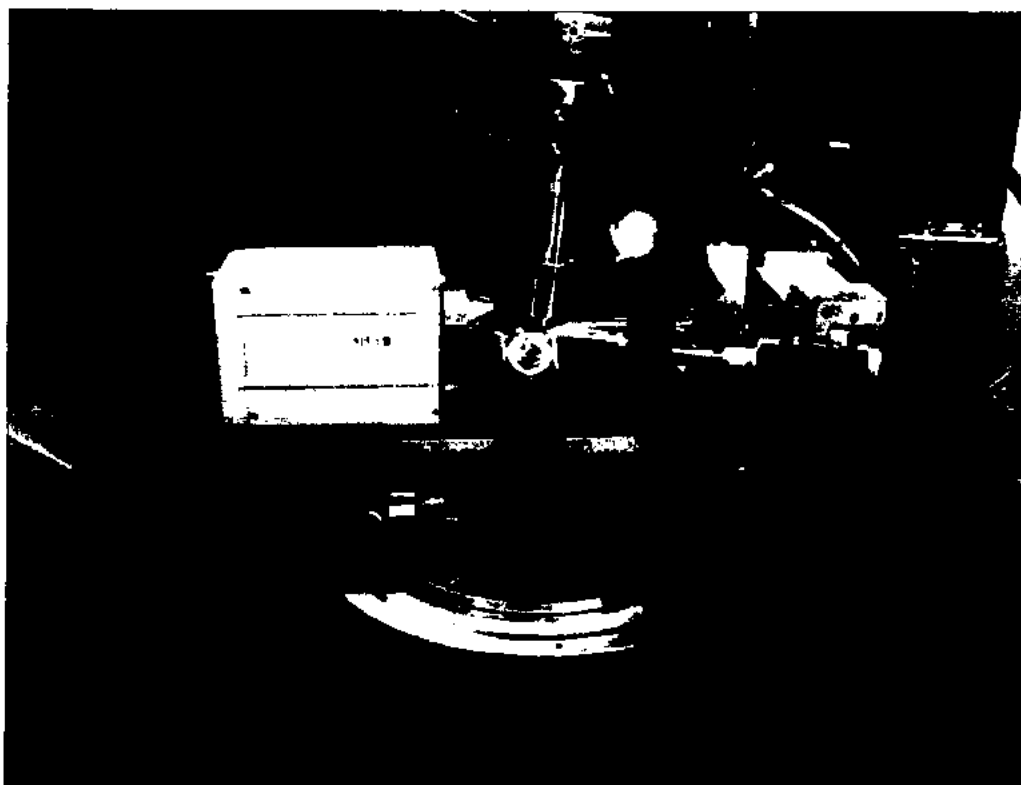
Fig. 3.3: X-ray diffractometer [46].

For focused and well-define beam, many collimators are placed within the path of beam. Then a filter is used to provide an approximate monochromatic beam. As soon as counter moves at certain angular velocity, a plot of intensities as function of 2θ is recorded automatically on the monitor. Schematic illustration of X-ray diffractometer is shown in Fig. 3.2.

3.1.3 Calculation of Average Crystallite size by Scherrer Formula

Suppose the thickness of some crystal is "t" and it is measured in a direction perpendicular to plane of reflection (Fig. 3.4). Consider a set of (m+1) plane under investigation. Let the variable quantity 'θ' as incident angle and θ_B as Bragg's angle, which satisfies the Bragg's condition for a certain values of inter-planner distance (d) and wave length (θ), i.e. $\theta = 2d\sin\theta_B$, the maximum intensity is obtained for m=1.

21
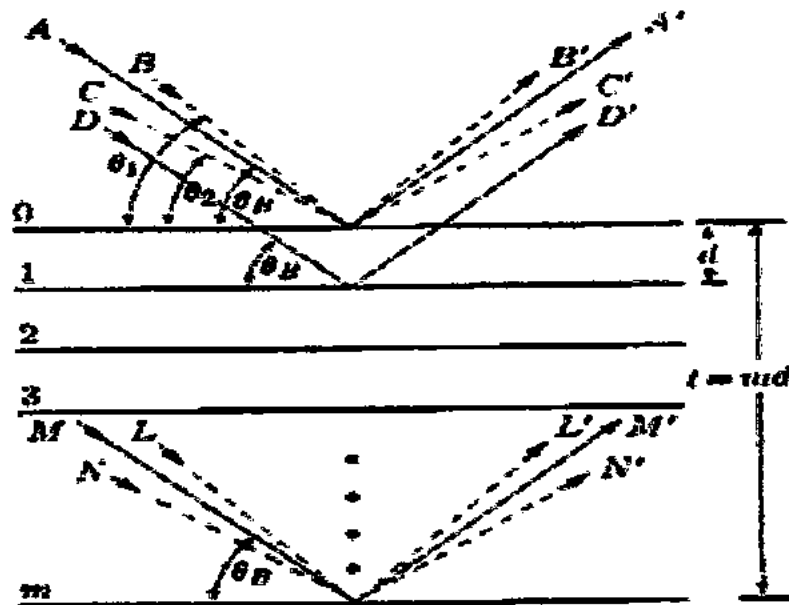
Fig. 3.4: Incident and reflected beams of X-ray from the crystallographic planes of crystal. The diffraction occurs at (θ_B's).

Now all the incident rays having Bragg's angle θ_B, reflecting at crystallographic planes with path difference $n\lambda$ i.e (integral multiple of wavelength) creates inference. Thus we get a constructive interference of all the reflected rays which are in same period and phase with each other. Those which are not in phase will interfere destructively and due to their low intensity will not be spotted at the detector. The plot for the recorded intensity verses 2θ will then has the form as shown in the Fig. 3.5(a) as compared to Fig. 3.5(b), which shows the theoretical case of diffraction only occurs at the exact Bragg angle 'θ_B'.
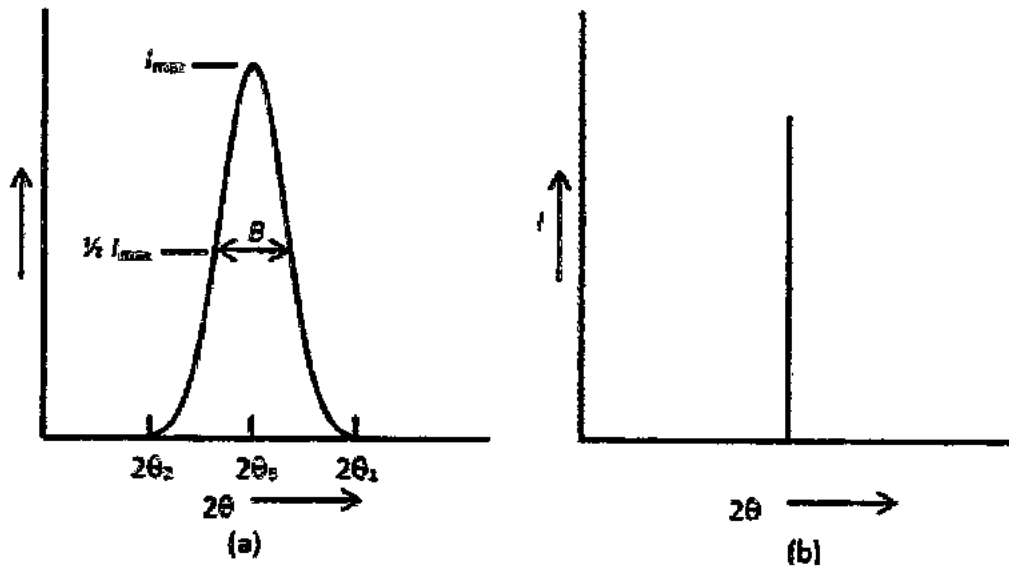
Fig. 3.5: Schematic representation of effect of particle size on diffraction curves.

Width of diffraction curve increases with the decrease of thickness of the crystal, as shown in the Fig. 3.5(a), this is because when value of m decreases, the range '$2\theta_1$-$2\theta_2$' increases. The width (β) is typically measured in radians at FWHM i.e. full width at half maximum. Note β is the angular width in double angle (2θ) and not in θ. As a rough estimate of β,

$$\beta = (\frac{2\theta_1 - 2\theta_2}{2}) = \theta_1 - \theta_2 \qquad (3.2)$$

Now take down the path-difference equation for the two angles such as θ_1 and θ_2,

$$2t\sin\theta_1 = (m+1)\lambda \qquad (3.3)$$

$$2t\sin\theta_2 = (m+1)\lambda \qquad (3.4)$$

Using the formula from Trigonometry and further solving the equation using small angle approximation,

$$t = \frac{\lambda}{\beta\cos\theta_B} \qquad (3.5)$$

A better representation is,

$$t = \frac{k\lambda}{\beta\cos\theta_B} \qquad (3.6)$$

23

Where k is 0.89 in our case, equation above is known as the Scherrer formula. It is used to calculate particle size of extremely small nanocrystals from the calculated values of XRD peaks [47].

3.2 Transmission Electron Microscope (TEM)

It is a technique, in which an electronic beam is transmitted through a very thin sample. This electronic beam intermingles with the specimen as it pass through it. Due to transmission of electrons, an image is formed, this image is then focused and modified on a fluorescent screen or it is to be spotted by sensor like a CCD camera.

TEMs resolution capability is significantly higher than light microscopes, because it uses electrons instead of light; also wavelength (de-Broglie wavelength) associated with electrons is very small. Due to this it is possible to observe the fine details even as small as a molecule of atoms, which is hundred times smaller than the object in a light microscope. Since the objects of the order of a few angstroms (10^{-10} m) can be viewed by TEM, so the details about the cell or different materials down to atomic level can be studied. Due to its high resolution and high magnification, TEM has become a valuable tool in the field of biological, medical, and materials research.

3.2.1 Principle of Operation

The working principle of the transmission electron microscope (TEM) is same as that of light microscope with only a difference that electrons are used instead of light. With an ordinary light microscope there is a limitation of wavelength of light and anything which is smaller than the wavelength of light cannot be seen in it. In transmission electron microscope the use of electron beam instead of light causes a resolution thousands times better than the light microscope (Fig. 3.6).
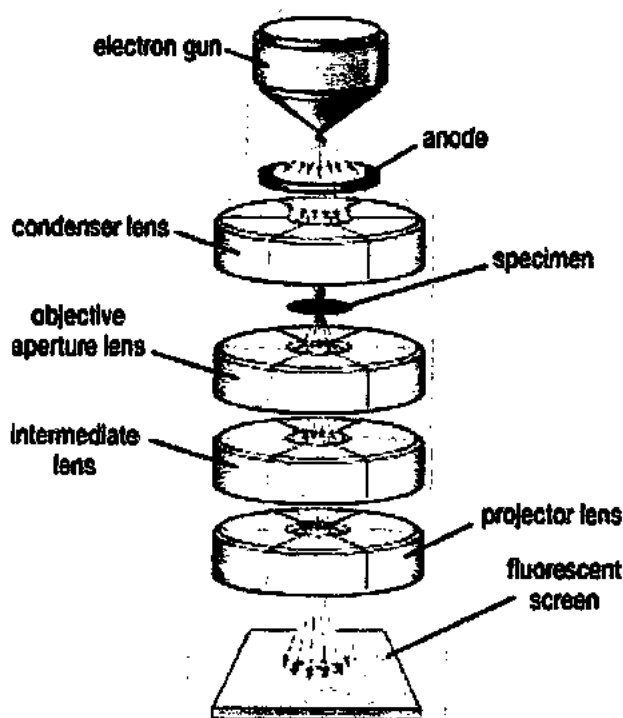
Fig. 3.6: Transmission electron microscope [48].

An "electron gun" emits the electrons which then travel though chamber of microscope. Electromagnetic lenses are used to direct the electrons into a beam. The electron beam then moves though the specimen which is under study. Some of the electrons will scatter after striking with the specimen but some of them transmit though it. At the bottom of the microscope un-scattered electrons hit the fluorescent screen which results in creation of "shadow image" of sample. Dark and bright areas are formed depending on density of a specimen. The image then can be photographed by camera or studied directly by the worker.

3.3 SQUID magnetometer

The detection coils shown in Fig. 3.7 consist of single piece of superconducting wire coiled in a set of three coils arranged such that upper coil is wound clockwise, middle anti-clockwise and the bottom as clockwise. Gradiometer arrangement is used to reduce noise in the detection circuit caused by fluctuations in the enormous magnetic field of the superconducting magnet. MPMS system works as superconducting magnet wound in a solenoidal arrangement. It's designed as to become a closed loop allowing to charge up to specific value and behave in persistent mode without the need of external power.

In order to take measurements, sample is moved cross the superconducting detection coils. These coils are situated at the center of magnet, outside the sample chamber. When the sample moves through the coils, magnetic moment of the sample changes, which induces an electric current in the detection coils. As the SQUID is designed to convert current- to-voltage, slight variation of current in detection coils causes variation in SQUID output voltage which is proportional to the magnetic moment of sample. Voltage variation from the detection coils of SQUID gives the information of magnetic moment of sample [49].

There are 3 different modes in which MPMS operates: hysteresis, oscillate, and no-overshoot. Firstly, in the no-overshoot mode, there is a monotonic change in magnetic field from initial to required field. In the oscillate mode the magnetic field value interchangeably overshoots and undershoots the required field with decreasing amplitude in every cycle. Finally, in the hysteresis mode the magnet is not in persistent mode and the current supply is constantly part of the magnet circuit.
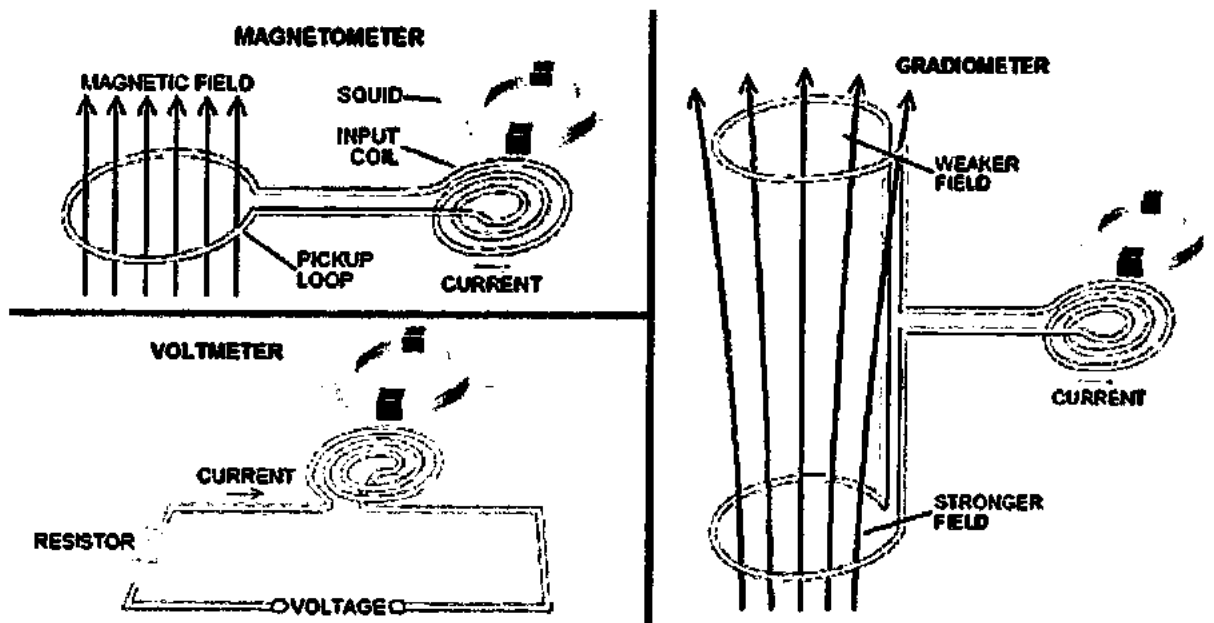

Fig. 3.7: Configuration of SQUID detection coils [49].

3.4 Measurements of Dielectric Properties

3.4.1 Sample preparation to measure dielectric properties

To measure the dielectric constant values of $CoCr_2O_4$ as a function of frequency, $CoCr_2O_4$ was used as a medium between plates of a parallel plate capacitor. For fabrication of the pallets 1g mass of the nanoparticles sample was pressed in a die under a pressure of $5ton/inch^2$. Pallets formed have got following diameter and thickness, as in Table 3.4

Table 3.4: Diameter and thickness of pallets used for dielectric properties.

SiO_2 Concentration	Diameter	Thickness
0%	13.28 mm	2.12 mm
45%	13.78 mm	4.00 mm
60%	13.90 mm	3.24 mm
80%	13.80 mm	3.33 mm

These pallets were then inserted in an electric furnace. Silver paste was applied in all sides. After this, pallets were placed in oven at 28°C for several hours in order to dry the silver paste completely. Copper wire leading from LCR meter was attached on the layer of silver paste for measurements.

3.4.2 Dielectric Properties Measurement

The dielectric properties of the all samples were measured by using IET 7600 LCR meter bridge. This was achieved by pressing the powder in disk shaped pallets under pressure. Silver paste was applied on both sides of the pallet which were then connected to the LCR meter through copper wire as shown in the Fig. 3.8. The experimental setup of the dielectric measurement were recorded at different frequency range 10 Hz-2 MHz i.e. capacitance and dissipation factor. The dielectric properties can be measured at different SiO_2 concentration with varying frequency. In the experimental setup first of all we set some specific frequency and then increased the voltage continuously and then recorded the reading on the LCR Meter.
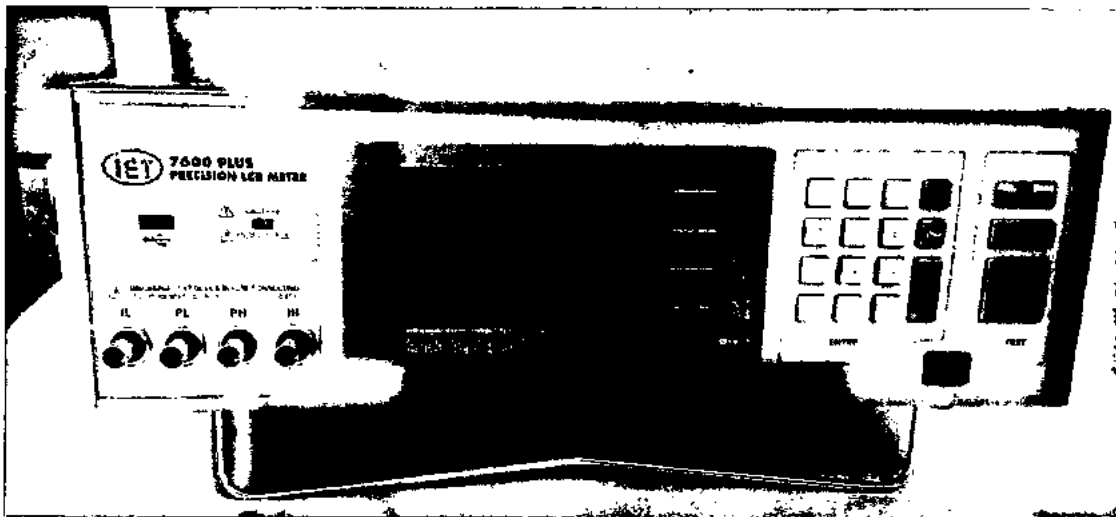
Fig. 3.8: Photograph of IET 7600 LCR Meter used for dielectric properties measurement.

3.4.3 Dielectric Constant

Dielectric constant is defined as "ratio of electric displacement D to the electric field intensity E", and a degree of a material to offer resistance to store a charge.

$$\epsilon = D/E \tag{3.7}$$

Physics behind the measurements of capacitance and dielectric constant of our sample is very simple, to understand the basic formalism, let us consider a parallel plate capacitor as shown in the Fig. 3.9.
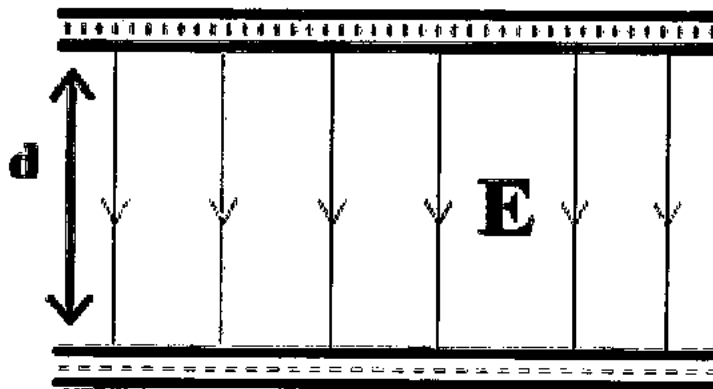

Fig. 3.9: Electric field in parallel plate capacitor.

Let A be the area of a plate of capacitor and d be the distance between the plates. Plates are connected to positive and negative terminals of the battery, as a result positive and negative charges

will accumulate on the plates respectively. Now these plates are just like two charged conducting sheets which generate electric fields. The electric field lines originate from positive plate and terminate at negative plate. So capacitance in the absence of dielectric is,

$$C = \frac{A}{d}\epsilon_0 \tag{3.8}$$

Capacitance in the presence of dielectric will be,

$$C' = A\epsilon_0\epsilon_r / d \tag{3.9}$$

In other words,

$$C' = \epsilon_r C \tag{3.10}$$

Where, ϵ_r is the relative permittivity of the material is given below,

$$\epsilon_r = Cd / A\epsilon_0 \tag{3.11}$$

ϵ_r can be calculated from LCR meter.

3.4.4 Dielectric Loss

The general expression of the capacitance in terms of dielectric is

$$C = A\epsilon\epsilon_0 / d \tag{3.12}$$

the loss tangent is defined as

$$tan\delta = \epsilon''/\epsilon' = 1/\omega RC \tag{3.13}$$

where

$$\omega = 2\pi f$$

R is equivalent resistance whereas C is capacitance and $tan\delta$ is a dielectric loss.

CHAPTER 4

Results and Discussion

4.1 X- Ray Diffraction Analysis

Fig. 4.1 shows the X-ray diffraction (XRD) pattern of the uncoated $CoCr_2O_4$ nanoparticles. All the indexed peaks correspond to spinel structure with no impurities. There are no diffraction peaks of SiO_2 matrix present due to its amorphouss nature.
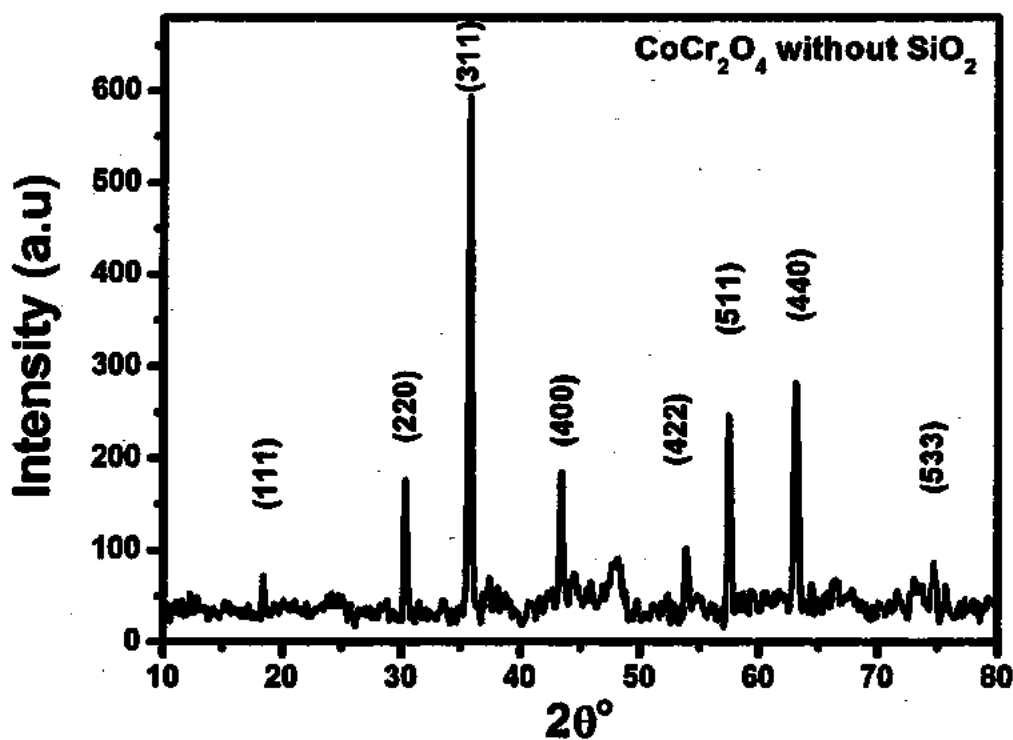
Fig. 4.1: XRD pattern of uncoated $CoCr_2O_4$ nanoparticles.

Fig. 4.2 shows the XRD patterns of the $CoCr_2O_4$ nanoparticles dispersed in $(SiO_2)_x$ matrix with x = 0%, 45%, 60% and 80%. The prominent Bragg peaks at scattering angle 2θ of 30.31, 35.70, 43.45, 57.40, and 63.04 degrees correspond to Miller indices (220), (311), (400), (511), and (440), respectively, of the cubic $CoCr_2O_4$ phase; JCPDS file no: 780711. The patterns could be indexed on the face-centered cubic cell with the Fd3m space group. The lattice parameter of the $CoCr_2O_4$ nanoparticles was found to be 8.348 Å, which is in agreement with the reported lattice

parameter in a literature i.e. $CoCr_2O_4$ (8.334 Å) [50]. It is worth stating here that no Bragg peaks corresponding to Cr_2O_3, Co_3O_4 or metallic cobalt were observed in the XRD pattern.
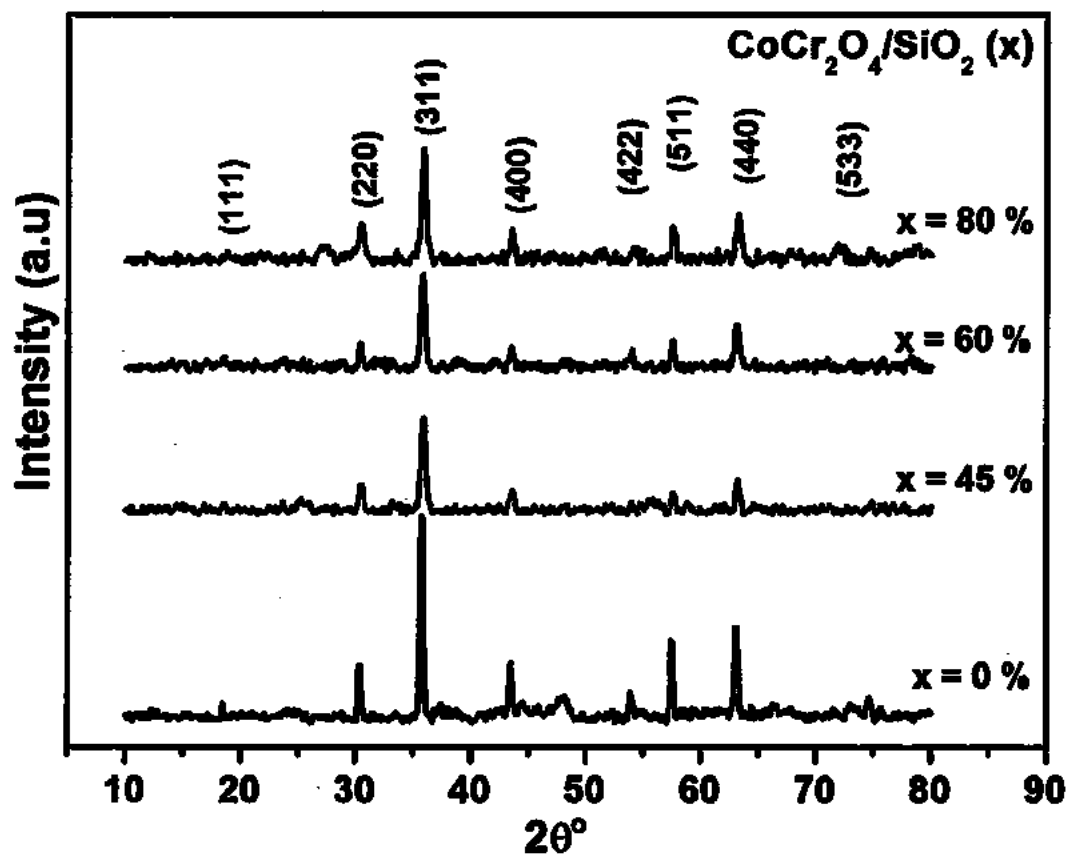
Fig. 4.2: XRD patterns of $CoCr_2O_4$ nanoparticles dispersed in $(SiO_2)_x$ matrix with x = 0%, 45%, 60% and 80%.

4.1.1 Effect of Silica on Average Crystallite size

Average crystallite size for $CoCr_2O_4$ was calculated for (111), (220), (311), (400), (422), (511) and (440) peaks respectively using Scherrer formula,

$$D = \frac{k\,\lambda}{\beta\cos\theta} \qquad\qquad (4.1)$$

where

k=0.91, Shape Factor

λ= 1.5406 Å (Wavelength of X-Rays for Cu Kα)

β= Line broadening at half the maximum intensity (FWHM) in radians

31

$\theta=$ Bragg's angle

$D=$ Mean size of particles

The average particle sizes for $CoCr_2O_4$ given below in the table 4.1

Table 4.1: Size calculation of cobalt chromite nanoparticles from XRD data.

Sample with SiO_2 Concentration	Crystallite size of peak (220)	Crystallite size of peak (311)
0%	65.23 nm	62.99 nm
45%	48.40 nm	41.81 nm
60%	47.62 nm	45.88 nm
80%	46.13 nm	37.68 nm

By knowing the broadening or reduction of a peak we can indicate the decrease or increase in size of a particle. Let's distinguish peak (311), here it's clearly shown that width of the peak is broad. It sharpens with the decrease in SiO_2 concentration. Similar thing happens with the peaks (400), (422), (511) and so on. The average crystallite size of the nanoparticles coated with 0, 45, 60, and 80% was 64.11, 45.10, 46.75 and 41.90nm respectively. Therefore average crystallite size of $CoCr_2O_4$ decreases with increase in SiO_2 matrix [51, 52].

4.1.2 XRD Assessment of Crystallite size vs Silica

To measure lattice parameter, crystallite size and phase formation, we used X-ray diffraction (XRD) having $CuK\alpha$ (0.154 nm) source at average temperature and pressure. Fig. 4.3(a) shows the XRD patterns of all SiO_2 coated $CoCr_2O_4$ nanoparticle samples with different values of SiO_2 concentration (x) =0, 0.45, 0.6 and 0.8. It has been perceived by using JCPDS reference card of XRD 780711 for $CoCr_2O_4$ and that all four samples have cubic spinel structure and don't have supplementary impurity of phase. Average crystallite size can be measured via Debye-Scherrer formula.
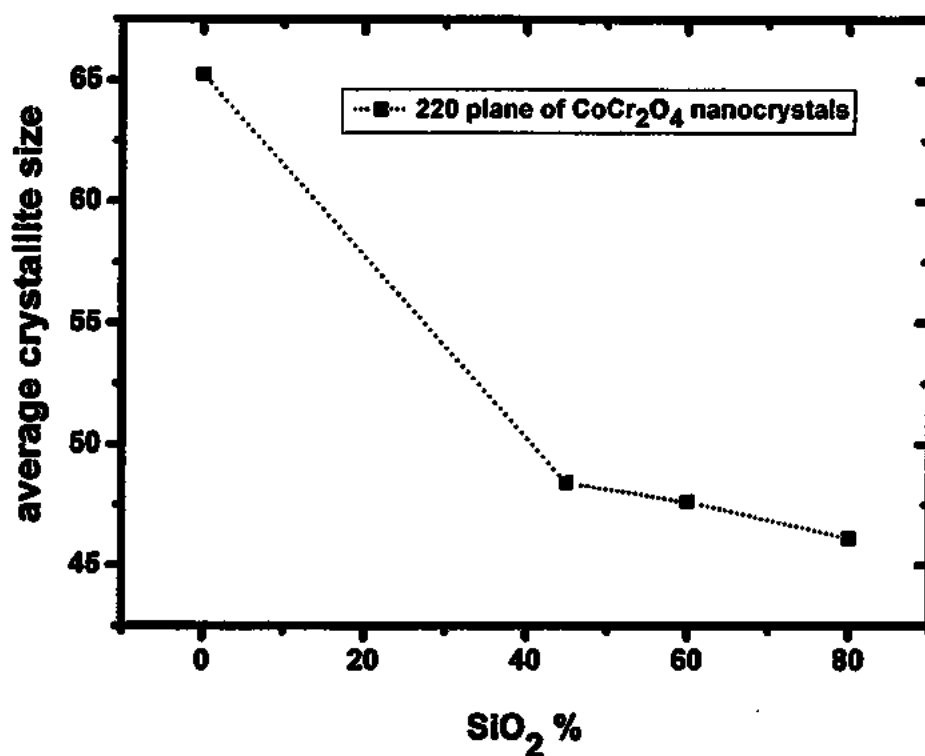
Fig. 4.3(a): Average crystallite size vs SiO_2 concentration.

Fig. 4.3(a) shows the variation of average crystallite size with SiO_2 concentration that falls in the range 46–64 nm.

4.1.3 Lattice Parameter and Crystal Structure

For the case of cubic crystal structure $CoCr_2O_4$ nanoparticles, the lattice parameters (a, b and c) can be calculated by using the relation, d^2_{hkl}

$$\frac{1}{d^2_{hkl}} = \frac{h^2 + k^2 + l^2}{a^2}$$

(4.2)

Where, 'd_{hkl}' is the inter planer spacing given by the Bragg's law $d=\lambda/(2\sin\theta)$ and h, k and l are the miller indices of the crystal planes. The reported values of the lattice parameters of $CoCr_2O_4$ are a = 8.371 Å. Our calculated values are a=8.315 Å, 8.285 Å, 8.3135 Å and 8.2958 Å using (220) plane for 0, 45%, 60% and 80% concentrations, respectively and have a good agreement with reported values. Fig. 4.3(b) shows variation of calculated values of lattice parameter of $CoCr_2O_4$ for different concentration of SiO_2. These lattice parameters show a cubic structure of $CoCr_2O_4$.
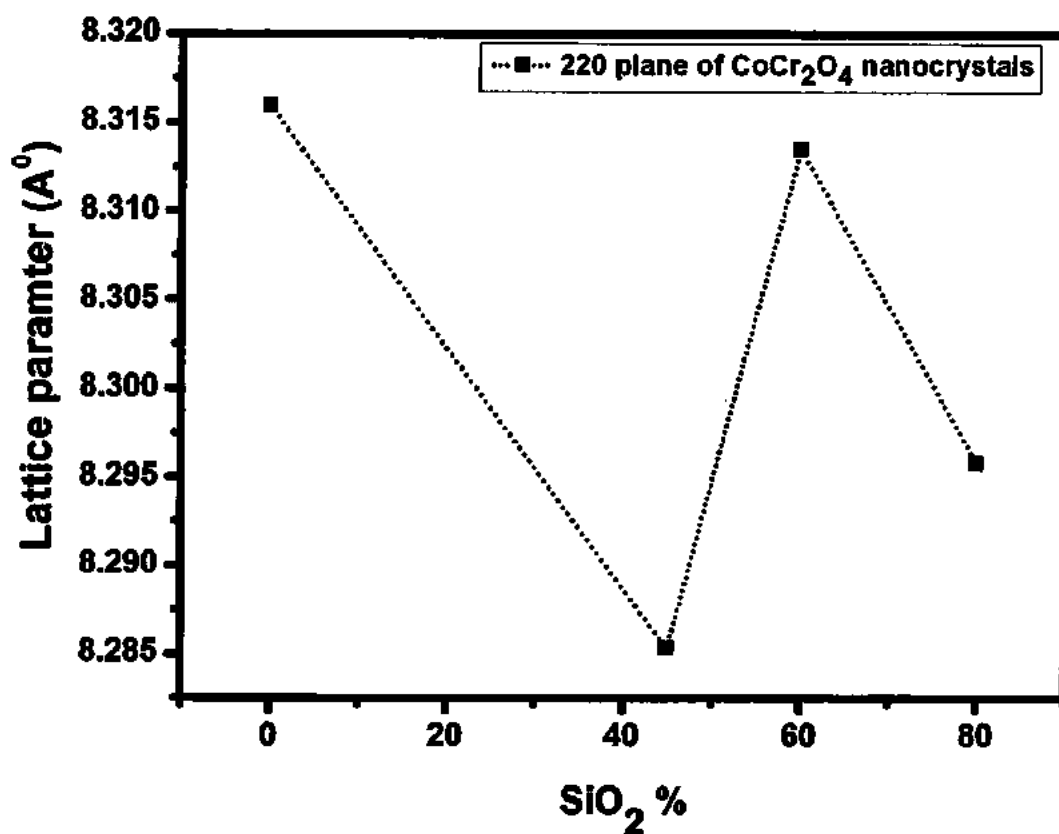
Fig. 4.3(b): Variation of lattice parameter of $CoCr_2O_4$ with different SiO_2 matrix.

4.2 Transmission Electron Microscopy

To observe the shape and structural properties of nanoparticles, transmission electron microscopy (TEM) was also used. Fig. 4.4 shows TEM for $CoCr_2O_4$ (0% SiO_2) nanoparticles at 110 nm scale. Well-developed edges of nanoparticles are formed. It is observed that crystallites have weak tendency to aggregate and quite well dispersed.

Fig. 4.4: TEM images of uncoated $CoCr_2O_4$ nanoparticles.

4.3 Temperature-dependent Magnetization

In Fig. 4.5, temperature-dependent magnetic properties of uncoated $CoCr_2O_4$ nanoparticles were measured using SQUID magnetometer. The magnetization curve of zero field cooled (ZFC) and field cooled (FC) for $CoCr_2O_4$ were observed under magnetic field of 50 Oe. The ZFC and FC data of $CoCr_2O_4$ reveal a ferrimagnetic transition at $T_c = 97$ K and conical spin transition at $T_s = 30$ K, which is good agreement with the values in literature for single and bulk crystals of $CoCr_2O_4$ [55, 56]. A clear kink at 30 K in FC curve which is associated with spiral magnetic order (T_s), is also called multiferroic phase (magnetic and electric dipoles at same phase) due to conical spin [57]. Above 100 K, the magnetization curves overlap and all samples show paramagnetic behavior. The magnetic behavior is significantly different below this temperature and the magnetization value is extremely dependent on the cooling regime used. Negative magnetization in ZFC data is also observed which is due to uncompensated spin at grain boundaries [58].
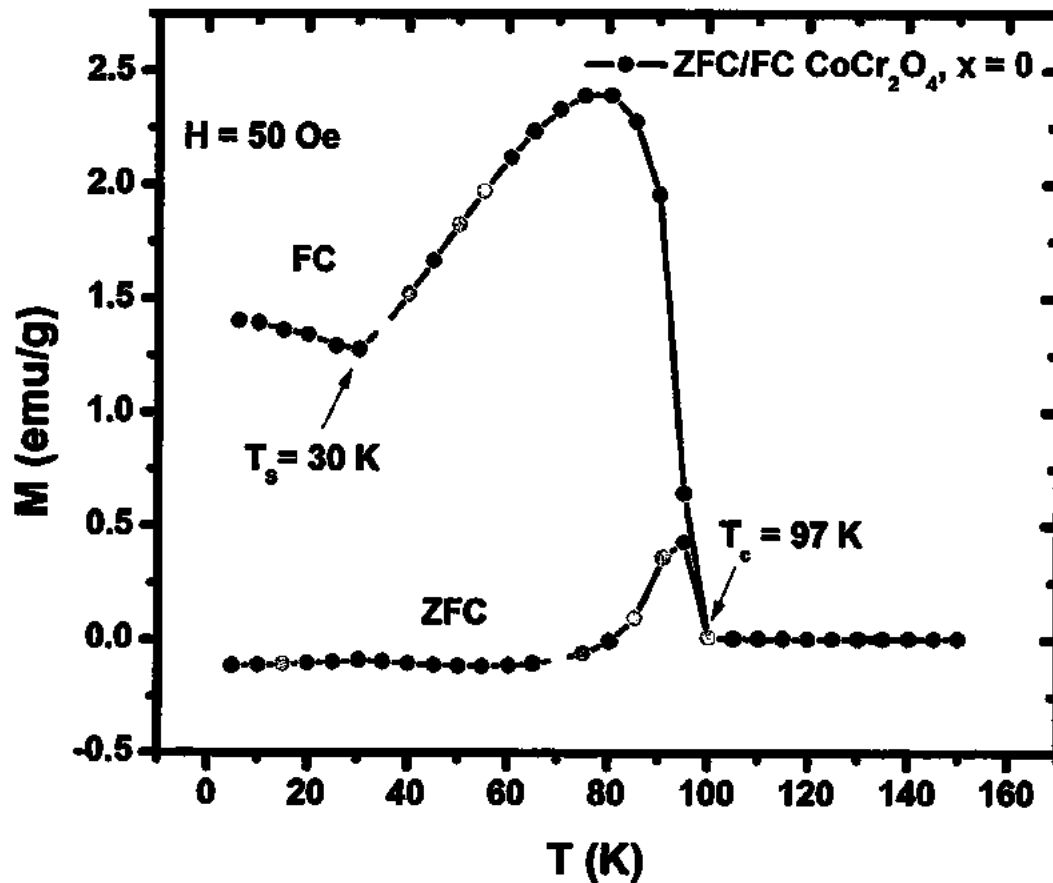
Fig. 4.5: ZFC/FC curves of uncoated $CoCr_2O_4$ nanoparticles.

4.4 Dielectric Properties

4.4.1 Real Part of Dielectric Constant (ε')

Measurements were done by using LCR meter in the frequency range of 10 Hz to 2 MHz at room temperature. Fig. 4.6 represents real part of dielectric constant of uncoated $CoCr_2O_4$ nanoparticles. It indicates that at low frequencies, dielectric constant is high while dielectric constant shows a decreasing trend with increasing frequency and becomes smooth at higher frequencies.
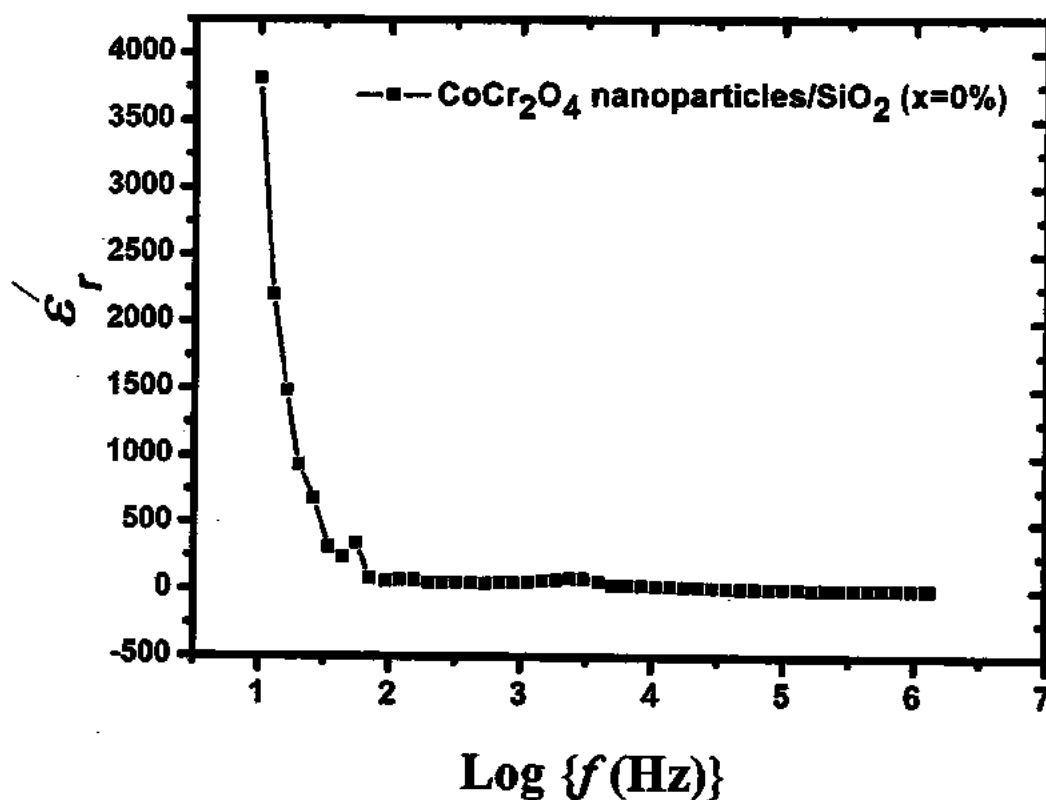
Fig. 4.6: Real part of dielectric constant of uncoated $CoCr_2O_4$ nanoparticles.

This behavior is common in chromites and ferrites [59]. To explain this lets get an example of Koop's model which consists of two layer model with grain and grain boundaries as conducing and restive layer, respectively. Electrons reach to non-conducting layer of grain boundary by hooping process in presence of electric field and due to high resistance electron piles up producing polarizations [60]. Dielectric constant decreases at higher frequency due to lagging of electrons and have difficulty to reach in required region (grain boundary).

Fig 4.7 shows real part of dielectric constant of $CoCr_2O_4$ samples with SiO_2 matrix (x=0%, 45%, 60% and 80%). At frequency f =100 Hz, real part of dielectric constant shows a non-monotonous behavior with a peak for x = 45% SiO_2 concentrated sample. At low frequency, 45% coated $CoCr_2O_4$ has maximum value of real part of dielectric constant. It decreases with the increase of frequency.
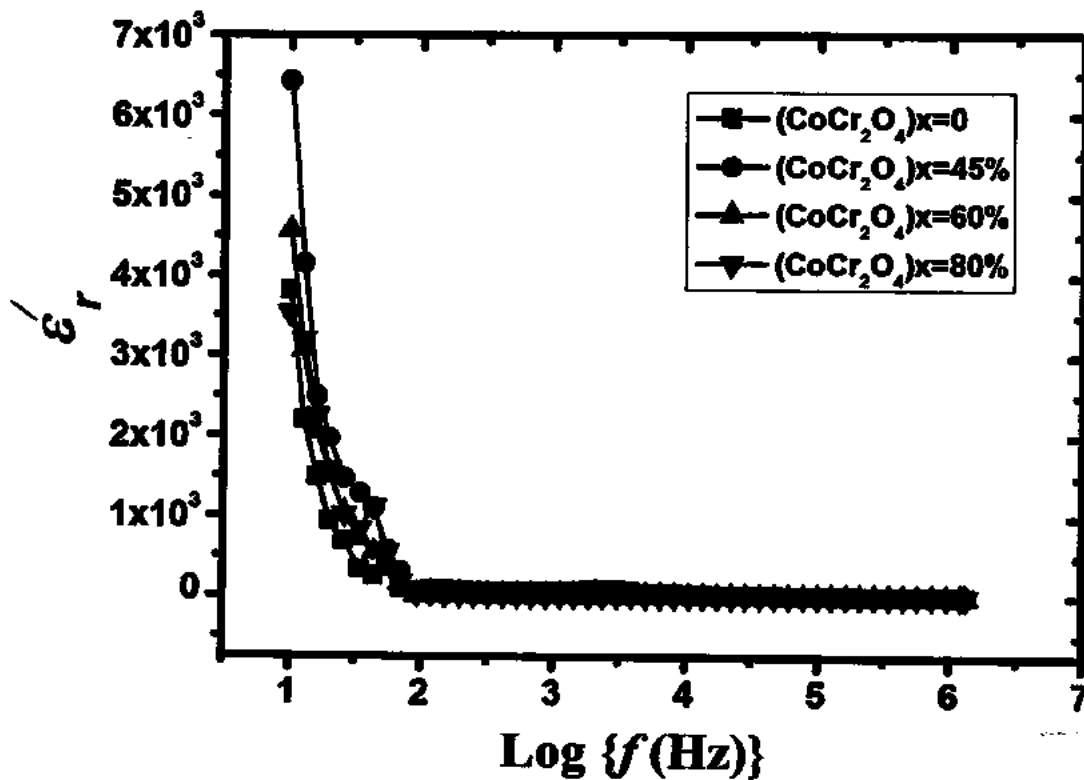
Fig 4.7: Real part of dielectric constant of $CoCr_2O_4$ nanoparticles with different SiO_2 concentrations (x=0%, 45%, 60%, and 80%).

Fig. 4.8 shows the variation of real part of dielectric constant of $CoCr_2O_4$ samples with SiO_2 matrix (x=0%, 45%, 60% and 80%). In the literature, it is reported that the dielectric constant usually decreases with increasing SiO_2 concentration but in our case, the dielectric constant shows non-monotonous behavior with maximum at 45% SiO_2 concentration. This might be due to crystallinity of the nanoparticles and change of polarization at 45% SiO_2 matrix concentration. Beyond 45%, dielectric constant decreases with increasing frequency,
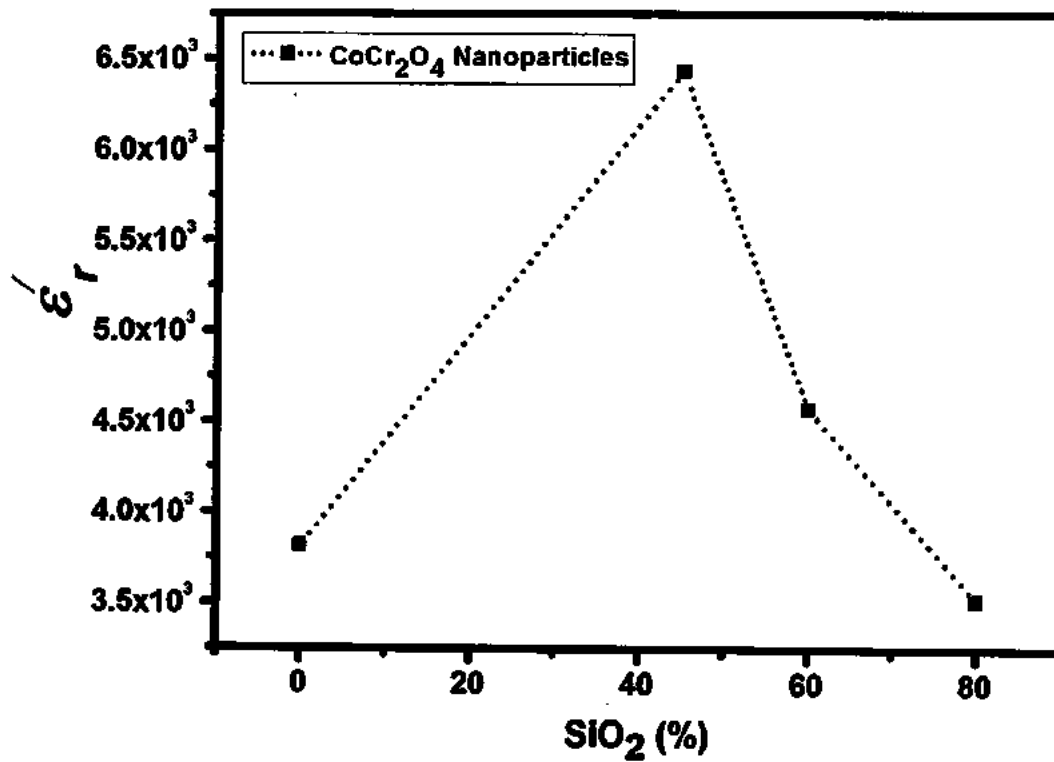
Fig. 4.8: Variation of real part of dielectric constant with SiO_2 concentration.

4.4.2 Imaginary Part of Dielectric Constant (ε'')

Fig. 4.9 shows the imaginary part of dielectric constant for uncoated $CoCr_2O_4$ nanoparticles. It indicates the typical behavior of chromites as we got for real part of dielectric constant for all the samples; large dielectric constant at low frequencies and vice versa.
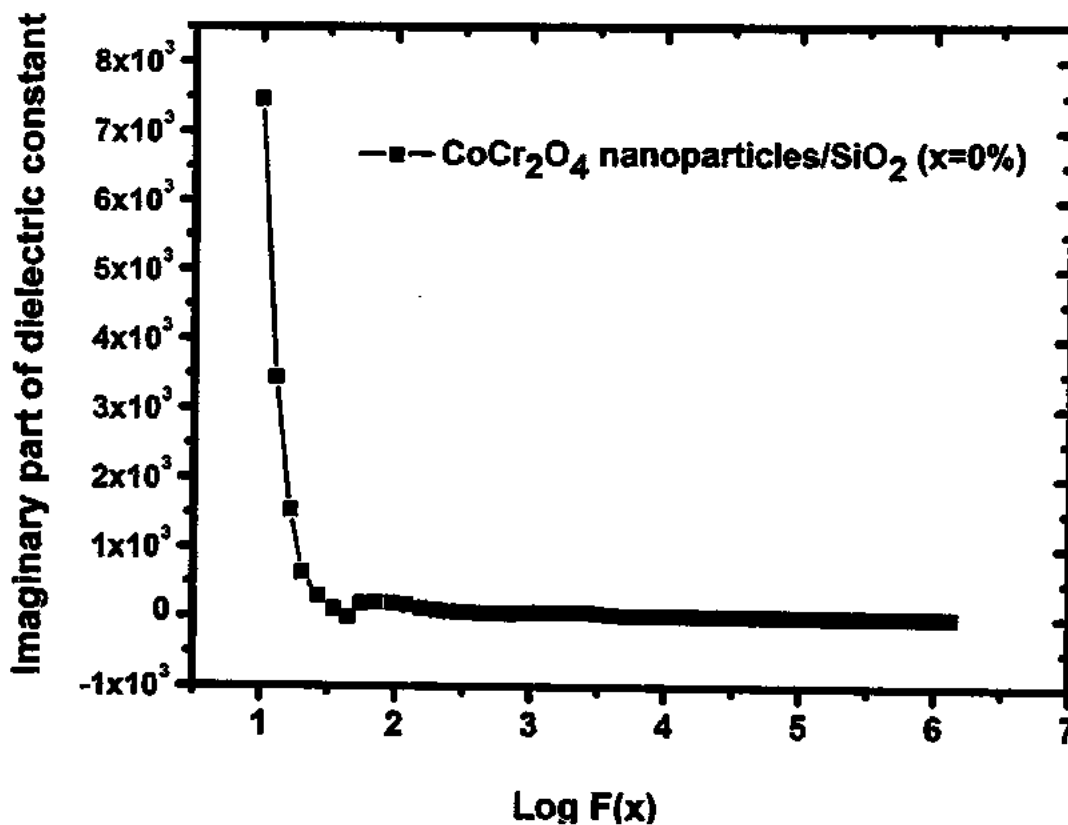
Fig. 4.9: Imaginary part of dielectric constant of uncoated CoCr$_2$O$_4$ nanoparticles.

Fig. 4.10 shows imaginary part of dielectric constant of CoCr$_2$O$_4$ samples with SiO$_2$ matrix (x=0%, 45%, 60%and 80%). It is also reported that imaginary part decrease with the increase of frequency. After certain frequency all the peaks come to same level and the behavior becomes smooth. Imaginary part depends on two factors that are real part and dissipation factor. Thus samples have greater values of imaginary part as compared to real part of dielectric constant. Polarization decreases with increase of frequency and dipoles do not depend on electric field at higher frequency [61].

Variation of imaginary part of dielectric constant (ε'') with frequency is shown in Fig. 4.10 This variation of dielectric constant with frequency can be explained by the fact that chromites are formed by agglomeration of newly born grains which are separated by thin poorly conducting transitional grain boundaries [62].
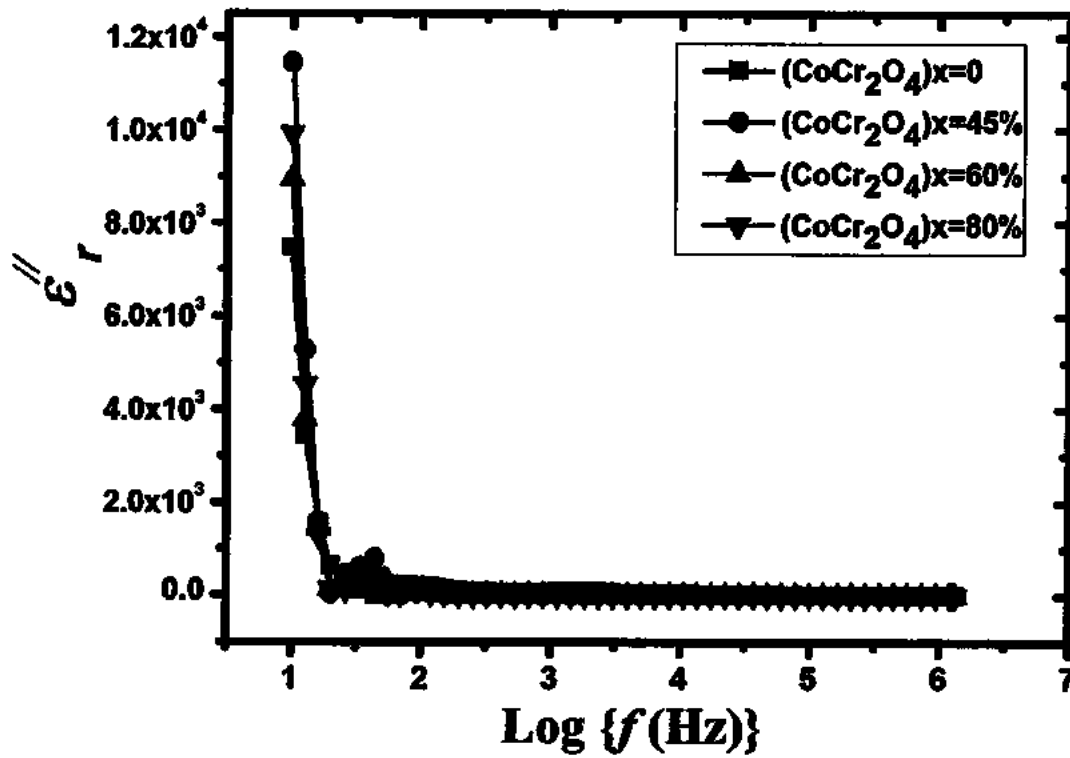
Fig. 4.10: Imaginary part of dielectric constant of $CoCr_2O_4$ samples with different SiO_2 concentrations.
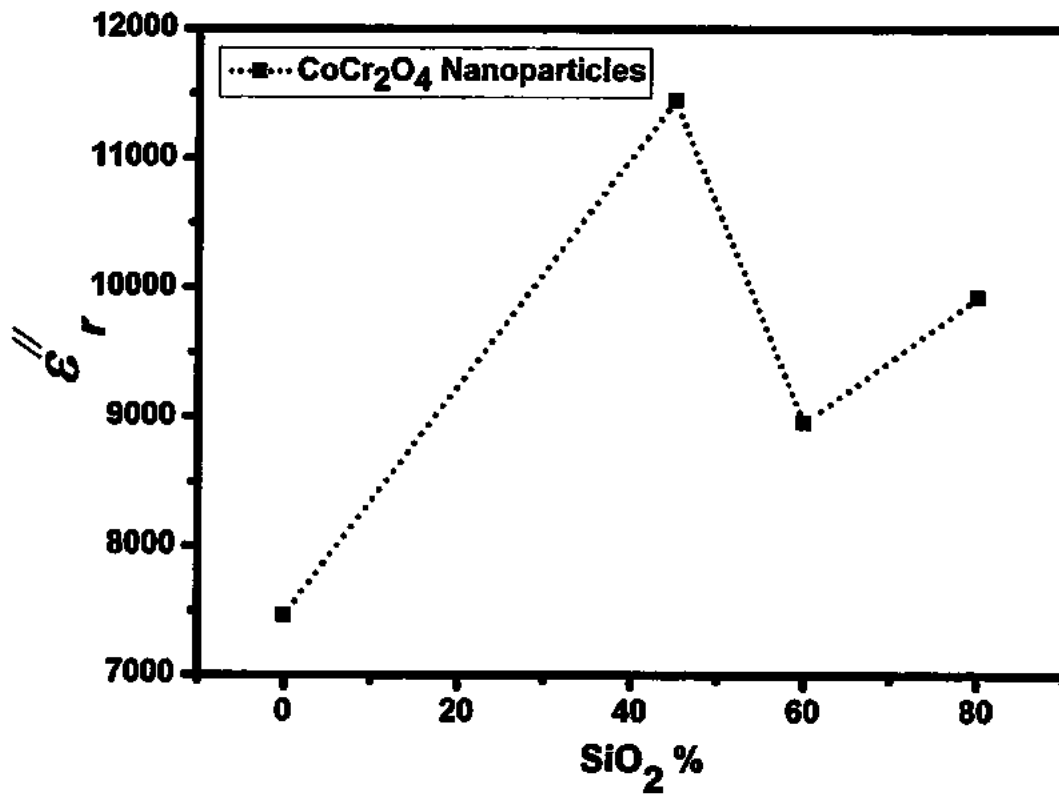

Fig. 4.11: Variation of Imaginary part of dielectric constant with SiO_2 matrix.

Fig. 4.11 represents the variation of imaginary part of dielectric constant (ε'') with SiO_2 concentration. Imaginary part of dielectric constant shows a non-monotonous behavior with increasing SiO_2 concentration for x = 45% SiO_2 concentrated sample. This is also attributed to phase and change of crystallinity of the nanoparticles as discussed for real part of dielectric constant. Furthermore, imaginary part decreases for 60% concentration and finally rises for 80% concentrated SiO_2.

4.4.3 Dielectric Loss Tangent
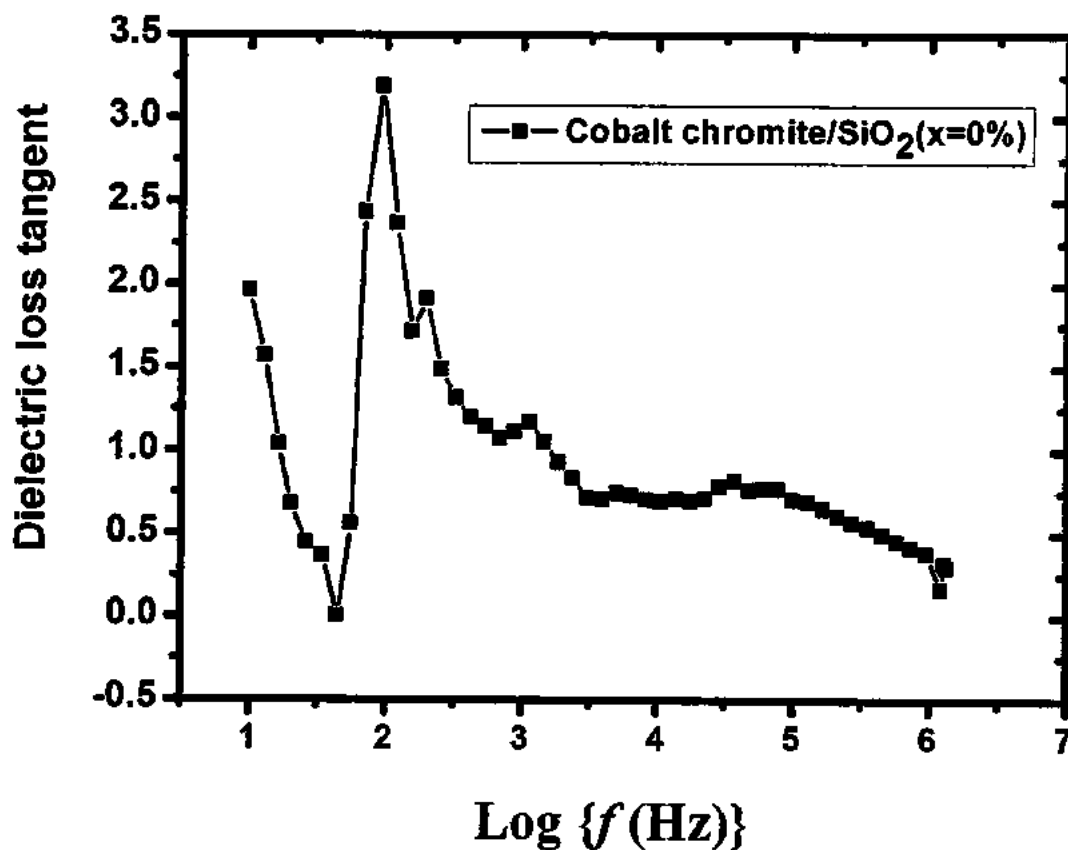
Fig. 4.12: Dielectric loss tangent (tanδ) of uncoated $CoCr_2O_4$ nanoparticles.

Fig. 4.12 shows dielectric loss tangent as function of frequency for uncoated $CoCr_2O_4$ nanoparticles. Fig. 4.13 shows dielectric loss tangent as function of frequency for $CoCr_2O_4$ nanoparticle samples with different concentrations of SiO_2 matrix (x = 0%, 45%, 60% and 80%). All the samples show nearly the same trend i.e. decrease of dielectric loss tangent at high frequencies. Although it demonstrate that the dielectric loss decreases with increasing SiO_2 concentration yet when dipoles are aligned in direction of electric fields, they get in such a way that they resist each other which results in dissipation of energy. Thus, by increasing concentration

42

of SiO_2, particle size decreases and hence dipole is reduced which result in decrease of dielectric loss tangents.

Fig. 4.13: Dielectric loss tangent of $CoCr_2O_4$ samples with different SiO_2 concentrations (x=0%, 45%, 60%, 80%)
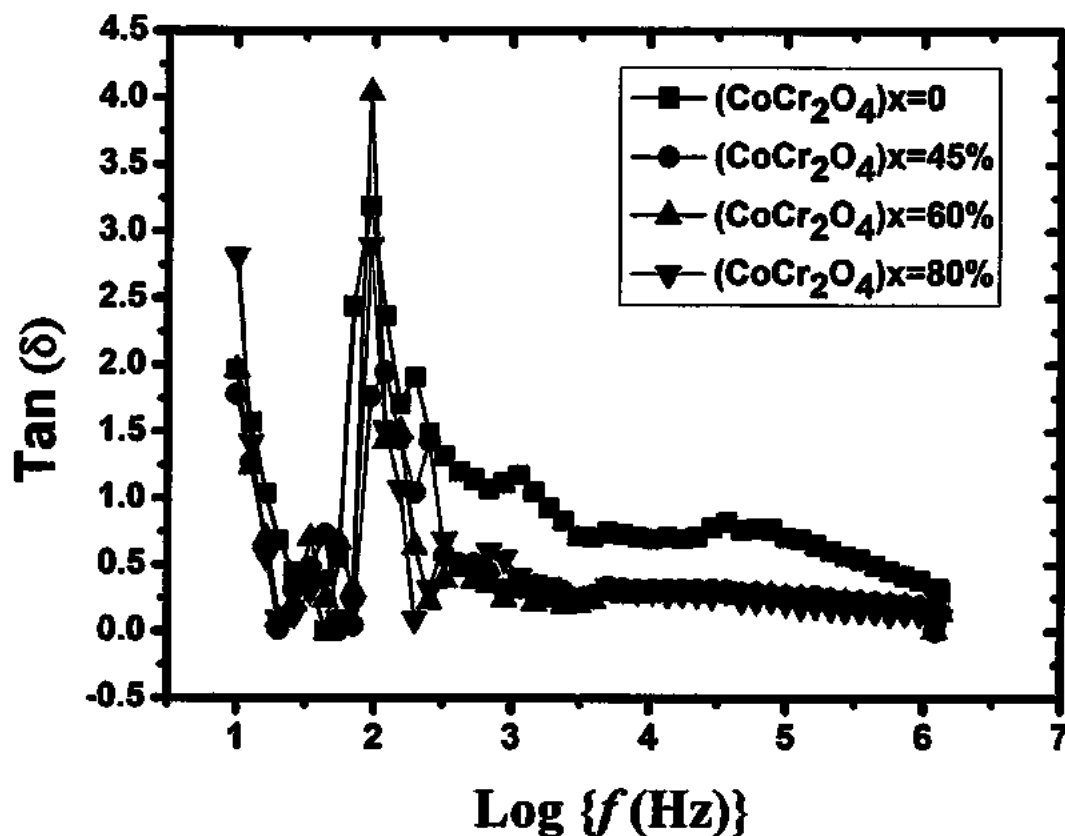
With the increase in frequency the loss factor decreases from 2.0 to 0, then it fluctuate at 0.5 and finally increases till 4.0. The values of tan δ rely upon many factors for instance, Cr^{2+} content, stoichiometry and structural homogeneity, that further depend on the sintering temperature and composition of the samples. [63] At lower frequency all the sample shows the dispersion in tan δ. The maximum loss peak occurs for the sample 60%, lowest of all is 45% sample. Except 0% sample, all the peaks become constant at higher frequencies. The reason behind constant value of tan δ is that, when frequency is increased further than a point reach where electric field reverses its direction and space charge do not contribute in polarization [64].

At frequency above 100 Hz there occurs resonance, this behavior can be explained as: when the frequency of external applied electric field is equal to hoping frequency of electrons, a peak is obtained in the loss tangent and it is called as the tangent resonance. Same behavior was observed

43

in many ferrites [65, 66]. Variation of loss tangent in contrast to SiO_2 percentage increases with the increase in SiO_2 concentration, visible in Fig. 4.14. The increasing trend of dielectric loss tangent is similar to the behavior reported previously in case of ferrites [67-68].
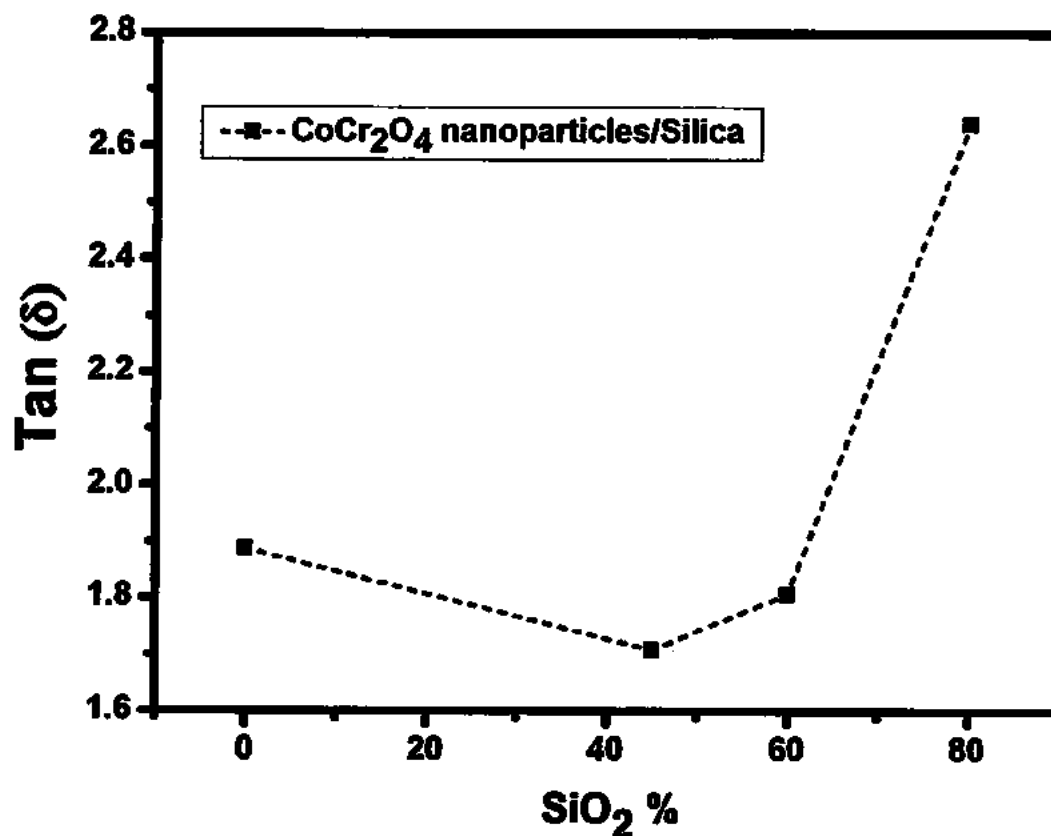
Fig. 4.14: Variation of dielectric loss tangent with SiO_2 concentration, dashed line just shows the trend.

4.4.4 AC Conductivity Measurements

The AC conductivity σ_{ac} measurements of all samples were carried out on the basis of dielectric data, it was obtained by using the dielectric constant (ε') and dielectric loss (tan δ) in the equation given below [69].

$$\sigma_{ac} = \varepsilon' \ \varepsilon_0 \omega \tan \delta,$$

Where ω is the angular frequency and ε_o the vacuum permittivity.

4.4.4.1 AC Conductivity Measurements for $CoCr_2O_4$

The AC conductivity measurements as a function of frequency was taken with the help of home-made two probe system and LCR meter. The plots of different samples are shown in Fig 4.15.
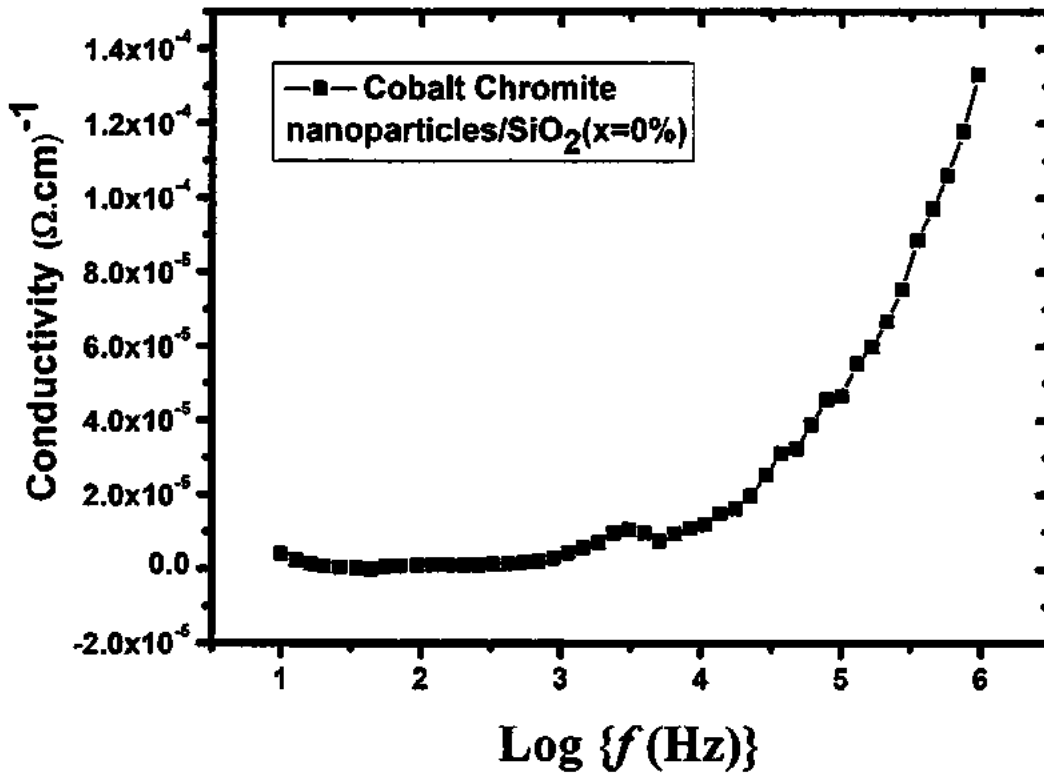
Fig. 4.15: AC conductivity of uncoated $CoCr_2O_4$ nanoparticles.

Fig. 4.16 shows AC conductivity as a function of frequency (Log f) for $CoCr_2O_4$ nanoparticles with different SiO_2 concentration (x= 0, 45%, 60% and 80%). It can be seen that plots show very consistent behavior at high and low frequencies, there is a slow initial increase followed by a rapid; exponential like increase. However in the case of high frequency data, that increasing trend is very swift. We also noticed that the value of conductivity in case of high frequency data is in general almost twice as that of the low frequency data.

Comparatively uncoated $CoCr_2O_4$ retain most AC conductivity as compared to other concentrations 45%, 60% and 80%. Moreover, SiO_2 coated $CoCr_4O_4$ nanoparticles have lower AC conductivity and it further decreases with increasing concentration as shown in Fig. 4.17. Lowest conductivity among all the samples is of 80%.

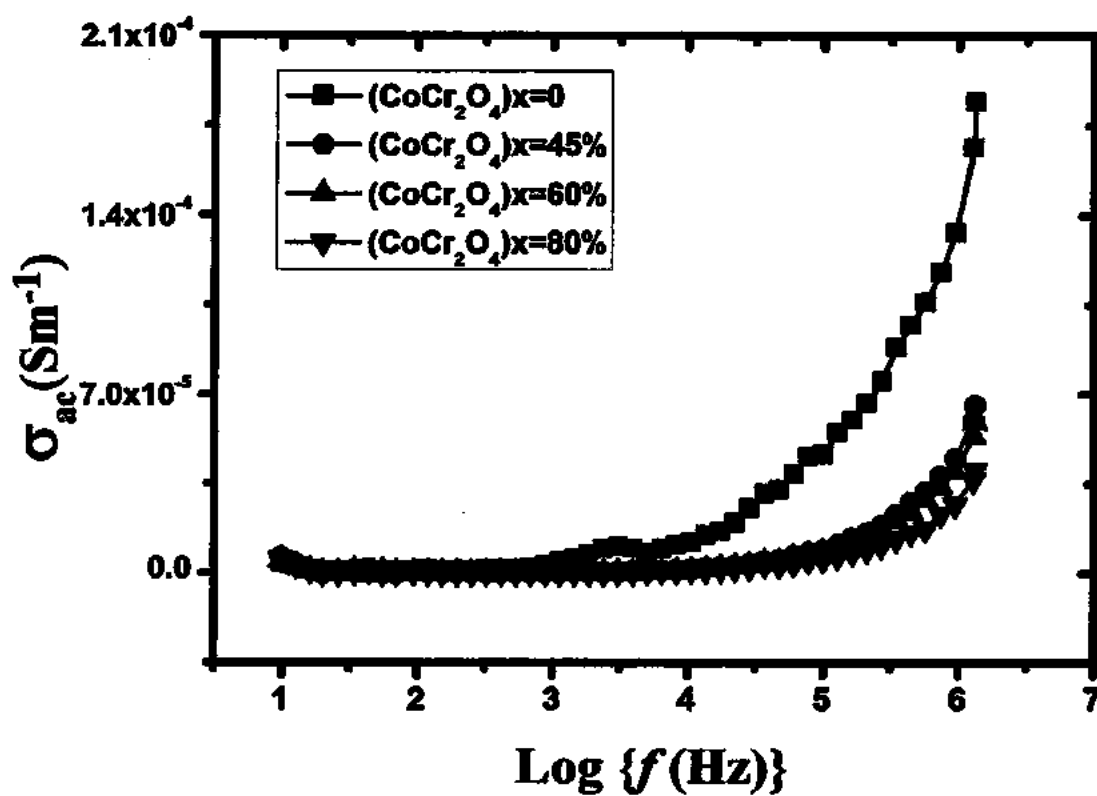**Fig. 4.16:** AC conductivity of $CoCr_2O_4$ samples with different SiO_2 concentrations (x=0%, 45%, 60% and 80%).

Fig. 4.17 shows variation of AC conductivity in contrast to SiO_2 percentage, it decreases with increasing SiO_2 concentration. This decreasing behavior of ac-conductivity is due to decrease in mobility of charge carriers.
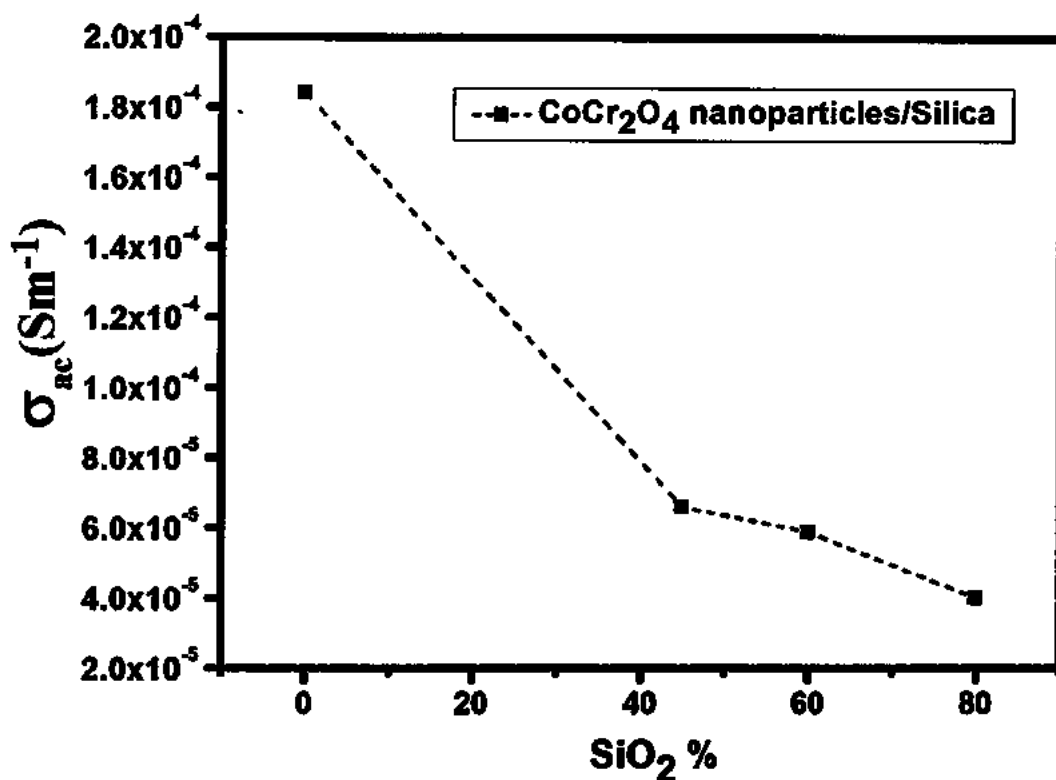
Fig. 4.17: Variation of AC conductivity with SiO_2 concentration.

4.5 Summary and Conclusion

To conclude, core shell nanoparticles consisting of a shell of SiO_2 and magnetic core of cobalt chromite ($CoCr_2O_4$) is synthesized by sol–gel process using tetraethyl ortho silicate (TEOS). The structure of core shell is confirmed by TEM. The dielectric properties of these nanocomposites are measured by LCR meter in ordinary temperature and in different SiO_2 matrix content ($CoCr_2O_4$ /$(SiO_2)_x$: x =0, 0.45, 0.6 and 0.80). Room temperature structural studies revealed that all the compositions exhibit single phase cubic structure. We optimized the annealing temperature to obtain samples with large dielectric constant comparable with literature. In the present work, optimization was carried out by studying effects of sintering temperature, electronic structure and dielectric properties for $CoCr_2O_4$ –SiO_2. Increase in SiO_2 concentration decreases the size of nanoparticles. Optimization reveals that pallets synthesized at 900°C have identical crystal and electronic structure. However change in temperature may change the crystal structure. The inter-planer distance calculated from TEM and XRD studies were found to be highly correlated with each other. XRD reveals the spinel structure of the nanoparticles. It is observed that crystallite size decreases with increasing concentration of SiO_2 matrix. Lattice parameter of the $CoCr_2O_4$

nanoparticles is also affected by SiO_2 concentration. It shows a decreasing trend with increasing SiO_2 matrix or with decreasing particle size. TEM micrographs indicates that the nanoparticles are nearly spherical in shape and non-agglomerated. Dielectric properties of $CoCr_2O_4$ attribute to diminishing of the particle size with increasing SiO_2 concentration. Smaller nanoparticles exhibit low dielectric constant values as compared to bulk due to the presence of the disordered and frustrated surface spins. The thickness of the surface spin layer increases with decreasing particle size because of large surface to volume ratio in smaller nanoparticles. In conclusion, SiO_2 matrix has dominant effects on structural and dielectric properties of $CoCr_2O_4$ nanoparticles.

4.6 References

1. A. H. Morrish, *The physical Principles of Magnetism*, J. Wiley and Sons Inc., (1965).

2. https://en.wikipedia.org/wiki/Ferromagnetism

3. N. Ida, *Engineering Electromagnetics*, 3rd Edition, 544, (2000).

4. B. D. Cullity, and C. D. Graham, *Introduction to Magnetic Materials*, 2nd Edition, Wiley-IEEE Press, (2011).

5. S. Malhotra, *Target physics*, Tata McGraw hill education private limited **229**, (2011).

6. J. S. Smart, *the Néel Theory of Ferrimagnetism*, American Journal of Physics **23(6)**, 356-370, (1955).

7. L. Néel, *Propriétées magnétiques des ferrites; Férrimagnétisme et antiferromagnétisme*, Annales de Physique (Paris) **3**, 137–198, (1948).

8. http://www.winnerscience.com/wp-content/uploads/2011/07/Figure-Polarization-300x188.png.

9. D. J. Griffiths, *Introduction to Electrodynamics*, 3rd Edition, prentice Hall, New Jarsey, USA, (1999).

10. C. Toumey, *Apostolic Succession: Does Nanotechnology Descend from Richard Feynman's 1959 Talk?* , Engineering & Science **68(1)**, 16-23, (2005).

11. N. Taniguchi, *On the Basic Concept of Nano-Technology*, Proc. Intl. Conf. Prod. Eng. Tokyo, Part II, Japan Society of Precision Engineering, (1974).

12. C. Q. Sun, B. K. Tay, S. Li, X. W. Sun, S. p. Lau, and T. p. *Chen, Bandgap expansion of a nanometric semiconductor*, Material Physics and Mechanics **4**, 129, (2001).

13. V. Kumar, A. Rana, M. S. Yada, and R. P. Pant, *Size-induced effect on nano-crystalline $CoFe_2O_4$*, Journal of Magnetism and Magnetic Materials **320**, 1729-1734, (2008).

14. J. N. Tiwari, R. N. Tiwari, and Kwang S. Kim, *Zero-dimensional, One-dimensional, Two-dimensional and Three-dimensional Nanostructured Materials for Advanced Electrochemical Energy Devices*, Progress in Materials Science **57**, 724–803, (2012).

15. G. Cao., *Nanostructures and Nanomaterials*, Imperial College Press, London, (2004)

16. https://en.wikibooks.org/wiki/Cell_Biology/Introduction/Cell_size

17. C. Rath, P. Mohanty, and A. Banerjee, *Magnetic properties of nanoparticles of cobalt chromite, Journal of Magnetism and Magnetic Materials* **323**, 1698–1702, (2011).

18. S. Krupika, and P. Novak, *In Ferromagnetic Materials*, edited by E. P. Wolfarth North-Holland, Amsterdam **3**, 189, (1982).

19. K. R. Choi, S. J. Kim, B. W. Lee, and C. S. Kim, *Bond frustration effect of Cr ions in magnetiochromite by Mössbauer spectroscopy*, Journal of Applied Physics **103**, 07B734, (2008).

20. L. Q. Yan, W. Ren, J. Shen, Z. H. Sun, and F. W. Wang, *The exchange biaslike effect in tetrahedral spinels $Cu_{1-x}Zn_xCr_2O_4(x=0.1,0.3)$*, Journal of Applied Physics **105**, 07A719, (2009).

21. J. Shen, L. Q. Yan, J. Zhang, F. W. Wang, J. R. Sun, F. X. Hu, C. B. Rong, and Y. X. Li, *Magnetic properties and magnetic entropy change in spinels $(Cd,M)Cr_2S_4$ with $M=Cu$ or Fe*, Journal of Applied Physics **103**, 07B315, (2008).

22. A. Broese Van Groenou, P. F. Bergers, and A. L. Stuyts, *Magnetism, microstructure and crystal chemistry of spinel ferrites*, Material Science and Engineering **3**, 317, (1969).

23. Y. Yafet and C. Kittel, *Antiferromagnetic Arrangements in Ferrites*, Physical Review **87**, 290 (1952).

24. T. A. Kaplan, *Classical Spin-Configuration Stability in the Presence of Competing Exchange Forces*, Physical Review **116**, 888, (1959).

25. T. A. Kaplan, K. Dwight, D. H. Lyons, and N. Menyuk, *Classical Theory of the Ground Spin State in Spinels (Invited talk*, Journal of Applied Physics **32**, 13S ,(1961).

26. D. H. Lyons, T. A. Kaplan, K. Dwight, and N. Menyuk, *Classical Theory of the Ground Spin-State in Cubic Spinels*, Physical Review **126**, 540, (1962).

27. N. Menyuk, *Modern Aspects of Solid State Chemistry; edited by C. N. R. Rao Plenum*, New York, 1, (1970).

28. T. A. Kaplan and N. Menyuk, Philosophical Magazine, *Spin ordering in three-dimensional crystals with strong competing exchange interactions*, **87**, 3711, (2007); **88**, 279 (2008).

29. Y. Yamasaki, S. Miyasaka, Y. Kaneko, J. P. He, T. Arima, and Y. Tokura, *Magnetic Reversal of the Ferroelectric Polarization in a Multiferroic Spinel Oxide*, Physical Review Letter **96**, 207204, (2006).

30. Y. J. Choi, J. Okamoto, D. J. Huang, K. S. Chao, H. J. Lin, C. T. Chen, M. V Veenendaal, T. A. Kaplan, and S. W. Cheong, *Thermally or Magnetically Induced Polarization Reversal in the Multiferroic CoCr₂O₄*, Physical Review Letter **102**, 067601, (2009).

31. L. Khanna, and N. K. Verma, *Silica/potassium Ferrite Nanocomposite: Structural, Morphological, Magnetic, Thermal and in Vitro Cytotoxicity Analysis* **178**, 1230-1239, (2013).

32. M. Naeem, et al., *Effect of Reducing Atmosphere on the Magnetism of $Zn_{1-x}Co_xO$ ($0\leq x \leq 0.10$) Nanoparticles*, Nanotechnology, **17(10)**, 2675, (2006).

33. S. H. Xiao, K. Luo, and L. Zhang, *The Structural and Magnetic Properties of Cobalt Ferrite Nanoparticles Formed in situ in Silica Matrix*, Materials Chemistry and Physics **123**, 385-389, (2010).

34. K. Nadeem , M. Shahid, and M. Mumtaz , *Competing Crystallite Size and Zinc Concentration in silica coated cobalt ferrite nanoparticles*, Progress in Natural Science **24**, 199-204,(2014).

35. A. Chaudhury, M. Mandal, and K. Mandal, *Preparation and study of NiFe₂O₄/SiO₂ core-shell nanocomposites, Journal of Alloys and Compounds* **487**, 698-702, (2009).

36. S. Zhanga, D. Donga, Yu. Suia, Z. Liua, H. Wanga, Z. Qiana, and W. Sua, *Preparation of core shell particles consisting of cobalt ferrite and silica by sol–gel process*, Journal of Alloys and Compound, (2006).

37. D. Gingasua, I. Mindrua, and D. C. Culita, *Structural, magnetic and catalytic properties of cobalt chromite obtained through precursor method*, Materials Research Bulletin **62**, 52-64, (2015).

38. D. Zakutna, A. Repko, I. Matulkova, *hydrothermal synthesis and characterization of cobalt chromite nanoparticles*, Journal of Nanoparticles Res. **16**, 2251, (2014).

39. D. P. Dutta, J. Manjanna, and A. K. Tyagi, *Magnetic properties of sonochemically synthesized CoCr₂O₄ nanoparticles*, Journal of Applied Physics **106**, 043915, (2009).

40. K. Nadeem, F. Zeb, M. Azeem, M. Mumtaz, and M. Anis ur rehman, *Effect of amorphous silica matrix on structural, magnetic, and dielectric properties of cobalt ferrite/silica nanocomposites*, Journal of non-Crystalline Solids **400**, 45-50, (2014).

41. L. Poul, et al., *Synthesis of Inorganic Compounds (Metal, Oxide and Hydroxide) in Polyol Medium: A Versatile Route Related to the Sol-Gel Process*, Journal of Sol-Gel Science and Technology **26(1-3)**, 261-265, (2003).

42. M. Naeem, et al., *Effect of reducing atmosphere on the magnetism of $Zn_{1-x}Co_xO$ $(0 \leq x \leq 0.10)$ nanoparticles*, Nanotechnology **17(10)**, 2675, (2006).

43. D. Jezequel , et al, *Submicrometer zinc oxide particles: Elaboration in polyol medium and morphological characteristics*, Journal of Materials Research **10(01)**, 77- 83, (1995).

44. https://www.boundless.com/physics/textbooks/boundless-physics-textbook/atomic-physics-29/the-early-atom-185/x-ray-spectra-origins-diffraction-by-crystals-and-importance-694-6348/

45. www.spec2000.net/09-xrd.htm

46. http://pages.vassar.edu/jotanski/single-crystal-x-ray-diffraction/

47. A. L. Patterson, *The Scherrer Formula for X-Ray Particle Size Determination*, Physical Review **56(10)**, 978-982, (1939).

48. http://www.britannica.com/technology/transmission-electron-microscope

49. https://sites.google.com/site/squiddevices/home

50. D. P. Dutta, J. Manjanna, and A. K. Tyagi, *Magnetic properties of sonochemically synthesized $CoCr_2O_4$ nanoparticles*, Journal of Applied Physics **106**, 043915, (2009).

51. Y. Choi, J. Okamoto, D. Huang, K. Chao, H. Lin,and C. Chen, *Thermally or magnetically induced polarization reversal in the multiferroic $CoCr_2O_4$*, Physical Review Letters **102(6)**, 067601, (2009).

52. J. B. Silva, C. F. Diniz, J. D. Ardinson, A. I. C. Persiano, and N. D. S. Mohallem, *Cobalt ferrite dispersed in a silica matrix prepared by sol-gel process*, Journal of Magnetic Material **272-276**, E1851-E1853, (2004).

53. M. Edrissi, and A. R. Keshavarz, *Synthesis of Cobalt Chromite Nanoparticles by Thermolysis of Mixed Cr^{3+} and Co^{2+} Chelates of 2- Mercaptopyridin N-Oxide*, Nano-Micro Letters **4**, 83-89, (2012).

54. A. B. P Lever, *Inorganic electronic spectroscopy*, 2nd edition, Elsevier, Amsterdam, (1984).

55. C. Rath, P. Mohanty, and A. Banerjee, *Magnetic properties of nanoparticles of cobalt chromite*, Journal of Magnetism and Magnetic Materials **323**, 1698–1702, (2011).

References

69. J. C. Maxwell, *Electricity and Magnetism*, Oxford University Press, (1929).